Supporting Information

The helical structure enhances the stability of a chiral one-dimensional dysprosium phosphonate in solvent

Zhi-Min Zhai,[a‡] Zeng-shuai Yan,[b‡] Yan Xu,[a,e‡] Yaoyao Zhang,[c] Tinglian Yuan,[c] Hong-Ming Ding,[b*] Song-Song Bao,[a] Yu-qiang Ma,[d] Wei Wang,[c*] Li-Min Zheng[a*]

Experimental details

Materials and physical measurements

R- and *S*-1-phenylethylamine were purchased from Aldrich without further purification, and all the other starting materials were of reagent grade quality. *R*- or *S*-(1-phenylethylamino)methyl-phosphonic acid (pempH$_2$) was prepared according to the literature method.[1] Elemental analyses for C, N and H were determined with Elementar Vario Macro cube. Infrared spectra were measured on a Bruker TENSOR 27 IR spectrometer with pressed KBr pellets in the range of 400-4000 cm^{-1}. Thermogravimetric analysis (TGA) was performed on a Mettler-Toledo TGA/DSC STARe thermal analyzer in the range of 25-500 °C under a nitrogen flow at a heating rate of 10 ºC/min. Single crystals were used for data collections on a Bruker D8 Venture diffractometer using graphite-monochromated Mo-K*α* radiation (λ = 0.71073 Å). Powder X-ray diffraction (PXRD) data were recorded on a Bruker D8 ADVANCE X-ray powder diffractometer (Cu-K) at room temperature. The circular dichroism spectra were recorded on a JASCO J-720W spectropolarimeter using KBr pellets at room temperature. Scanning electron microscope (SEM) was carried out on Hitachi S-4800. The swelling and exfoliation experiments of crystals and helices were tested using a Nikon TiE inverted fluorescent microscope equipped with a Hamamatsu sCMOS camera. The stability experiments of nanofibers and helices were performed on Bruker Dimension ICON FastScan rapid atomic force microscope (AFM).

Synthesis crystals of *R*-Dy(*R*-pempH)$_3$·H$_2$O (*R*-1c)

A typical procedure for the preparation of ***R*-1c** is described as below. A mixture of Dy(NO$_3$)$_3$·6H$_2$O (0.1 mmol, 0.0456 g) and *R*-pempH$_2$ (0.5 mmol, 0.1080 g) in 9 mL of H$_2$O, adjusted to pH 3.7 with 0.5 mol/L NaOH, was kept in a Teflon-lined autoclave at 120 °C for 2 days. After cooling to room temperature, colorless rod-like crystals were obtained. Yield: 35.3% based on Dy. Elemental analysis calcd (%) for C$_{27}$H$_{39}$N$_3$O$_9$P$_3$Dy·H$_2$O: C 39.40, H 5.02, N 5.11; Found: C 39.92, H 4.99, N 5.09. IR (KBr, cm^{-1}): 3387(s), 2803(m), 2502(m), 2526(m), 2352(w), 1618(w), 1267(m), 1152(s), 1082(s),

1022(s), 989(s), 822(w), 763(m), 702(m), 565(m), 537(m), 473(w). Thermal analysis revealed that the weight loss below 110 °C was 2.67%, in agreement with the release of one lattice water molecules (calcd. 2.19%).

Synthesis crystals of *S*-Dy(*R*-pempH)$_3$·H$_2$O (*S*-1c)

Crystals of ***S*-1c** was obtained following the same procedure as for ***R*-1c** except that the *R*-pempH$_2$ was replaced by *S*-pempH$_2$. After cooling to room temperature, colorless rod-like crystals were obtained. Yield: 38.2% based on Dy. Elemental analysis (%) calcd (%) for $C_{27}H_{39}N_3O_9P_3Dy·H_2O$: C 39.40, H 5.02, N 5.11; Found: C 39.04; H, 5.04; N, 5.03. IR (KBr, cm^{-1}): 3387(s), 2981(s), 2791(s), 2514(w), 1618(m), 1460(s), 1385(w), 1274(m), 1151(m), 1084 (m), 1020(s), 987(s), 761(s), 701(s), 566(s), 537(s), 508(m), 474(w).

Synthesis helices of *R*-Dy(*R*-pempH)$_3$·H$_2$O (*R*-1h)

A typical procedure for the preparation of ***R*-1h** is described as below. A mixture of Dy(NO$_3$)$_3$·6H$_2$O (0.1 mmol, 0.0456 g) and *R*-pempH$_2$ (0.5 mmol, 0.1080 g) in 9 mL of H$_2$O, adjusted to pH 3.5 with 0.5 mol/L NaOH, was kept in a Teflon-lined autoclave at 120 °C for 2 days. After cooling to room temperature, colorless rod-like crystals were obtained. Elemental analysis calcd (%) for $C_{27}H_{39}N_3O_9P_3Dy·H_2O$: C 39.40, H 5.02, N 5.11; Found: C 38.97, H 5.36, N 5.13. IR (KBr, cm^{-1}): 3384(s), 2805(m), 2502(m), 2524(m), 2352(w), 1618(w), 1267(m), 1152(s), 1082(s), 1020(s), 989(s), 822(w), 761(m), 704(m), 566(m), 539(m), 474(w). Thermal analysis revealed that the weight loss below 110 °C was 2.33%, in agreement with the release of one lattice water molecule (calcd. 2.19%).

Crystallography

A suitable single crystal of ***R*-1c** was selected for indexing and intensity data collection on a Bruker SMART APEX CCD diffractometer using graphite-monochromatized Mo Kα radiation (λ= 0.71073 Å) at room temperature. The data were integrated using the Siemens SAINT program,[2] with the intensities corrected for Lorentz factor, polarization, air absorption, and absorption due to variation in the path length through the detector

face plate. Absorption corrections were applied. The structures were solved by direct methods and refined on F^2 by full-matrix least-squares using SHELXTL.[3] All the non-hydrogen atoms were located from the Fourier maps, and were refined anisotropically. All H atoms were refined isotropically with the isotropic vibration parameters related to the non-hydrogen atoms to which they are bonded. CCDC 2086980 for ***R*-1c** contain crystallographic data for this paper.

QCM measurements

The adsorption of chiral butanol in the QCM system was carried out under aqueous condition. The electrode was immersed in deionized water until the frequency stable first. Then, the *R*- or *S*-2-butanol solution (1 mM) was then injected at a flow rate of 100 μL min^{-1} till the signals tended to the stabilization again. The frequency change (Δf) was used to scale the mass of *R*- or *S*-2-butanol adsorbed onto the ***R*-1G**. The mass increase resulting from *R*- or *S*-2-butanol adsorption onto the resonator surface was estimated from the Sauerbrey equation,[4] using the following relationship between adsorbed mass ∆m (ng cm^{-2}) and frequency shift ∆*f* (Hz), by taking into account the characteristics of the resonators:

$$\Delta f = - C_f \Delta m \qquad (1)$$

where Δf is the change in fundamental frequency in Hz, Δm is observed mass change per unit area in g/cm^2 on quartz, C_f is the sensitivity factor of the crystal (56.6 Hz μg^{-1} cm^2 for a 5 MHz AT-cut quartz crystal at room temperature).

All-atom molecular dynamics simulations

The all-atom molecular dynamics (MD) simulations were performed using GROMACS 2020.6 package[5] with the Amber force field[6] and the TIP3P water model[7]. The General Amber force field[8] (GAFF) parameter for *R*-pempH$^-$, alkyl alcohols and halomethane were generated by AmberTools23[9]. Their RESP charge[10] were obtained through B3LYP/def2TZVP quantum calculations of the electrostatic potential using the Gaussian09 program[11] and fitted with Multifwn[12]. The parameter of Dy were obtained

from previous work of Merz's group[13]. The ***R*-1c** crystal used in MD simulation consists with seven chains and each chain consists with seven Dy atoms and twentyfour *R*-pempH$^-$. ***R*-1c** was solvated in a cubic box with 8×8×8 nm^3 and then Na^+ is added to neutralize the system. The system was energy-minimized by the steepest descent method until the convergence was reached. After the energy minimization, the system was equilibrated for 2.5 ns in the NVT ensemble, where the heavy atoms of ***R*-1c** were restrained using 1000 kJ mol^{-1} nm^{-2} harmonic constraints. Then, the 100 ns NPT simulations were performed with a time step of 2 fs. The pressure was maintained at 1 bar using the Berendsen barostat with a time constant of 2.0 ps, and the temperature was maintained at 298 K by the Berendsen thermostat with a time constant of 1.0 ps.[14] The Lennard-Jones interaction was computed using a cutoff of 1.2 nm, and the particle-mesh Ewald (PME) method was used to treat the long-range electrostatic (ELE) interactions[15]. The bonds involving hydrogen atoms were constrained by the LINCS algorithm[16]. Periodic boundary conditions were applied in all three directions.

References

[1] X.-G. Liu, S.-S. Bao, Y.-Z. Li, L.-M. Zheng. Polymorphism in homochiral zinc phosphonates. *Inorg. Chem.*, **2008**, *47*, 5525–5527.

[2] *SAINT*, Program for Data Extraction and Reduction, Siemens Analytical X-ray Instruments, Madison, WI, **1994–1996**.

[3] Sheldrick, G. M., *SHELXT* 2014/5, 2014; *SHELXL* 2018/3, **2018**.

[4] C. K. O'Sullivan, G. Guilbault. Commercial quartz crystal microbalances – theory and applications. *Biosens. Bioelectron.* **1999**, *14*, 663-670.

[5] M. J. Abraham, T. Murtola, R. Schulz, S. Páll, J. C. Smith, B. Hess, E. Lindahl, GROMACS: High performance molecular simulations through multi-level parallelism from laptops to supercomputers. *SoftwareX*, **2015**. *1*, 19-25.

[6] J. A. Maier, C. Martinez, K. Kasavajhala, L. Wickstrom, K. E. Hauser, C. Simmerling, ff14SB: improving the accuracy of protein side chain and backbone parameters from ff99SB. *J. Chem. Theory Comput.*, **2015**. *11*, 3696-3713.

[7] W. L. Jorgensen, J. D. Madura, Quantum and statistical mechanical studies of liquids. 25. Solvation and conformation of methanol in water. *J. Am. Chem. Soc.*, **1983**. *105*, 1407-1413.

[8] J. Wang, R. M. Wolf, J. W. Caldwell, P. A. Kollman, D. A. Case, Development and testing of a general amber force field. *J. Comput. Chem.*, **2004**. *25*, 1157-1174.

[9] D. A. Case, H. M. Aktulga, K. Belfon, D. S. Cerutti, G. A. Cisneros, V. W. D. Cruzeiro, N. Forouzesh, T. J. Giese, A. W. Götz, H. Gohlke, S. Izadi, K. Kasavajhala, M. C. Kaymak, E. King, T. Kurtzman, T.-S. Lee, P. Li, J. Liu, T. Luchko, R. Luo, M. Manathunga, M. R. Machado, H. M. Nguyen, K. A. O'Hearn, A. V. Onufriev, F. Pan, S. Pantano, R. Qi, A. Rahnamoun, A. Risheh, S. Schott-Verdugo, A. Shajan, J. Swails, J. Wang, H. Wei, X. Wu, Y. Wu, S. Zhang, S. Zhao, Q. Zhu, T. E. Cheatham III, D. R. Roe, A. Roitberg, C. Simmerling, D. M. York, M. C. Nagan, K. M. Merz Jr., AmberTools. *J. Chem. Inf. Model.*, **2023**. *63*, 6183-6191.

[10] C. I. Bayly, P. Cieplak, W. Cornell, P. A. Kollman, A well-behaved electrostatic potential based method using charge restraints for deriving atomic charges: the RESP model. *J. Phys. Chem.*, **1993**. *97*, 10269-10280.

[11] M. J. Frisch, G. W. Trucks, H. B. Schlegel, G. E. Scuseria, M. A. Robb, J. R. Cheeseman, G. Scalmani, V. Barone, B. Mennucci, G. A. Petersson, H. Nakatsuji, M. Caricato, X. Li, H. P. Hratchian, A. F. Izmaylov, J. Bloino, G. Zheng, J. L. Sonnenberg, M. Hada, M. Ehara, K. Toyota, R. Fukuda, J. Hasegawa, M. Ishida, T. Nakajima, Y. Honda, O. Kitao, H. Nakai, T. Vreven, J. A. Montgomery, J. E. P. Jr., F. Ogliaro, M. Bearpark, J. J. Heyd, E. Brothers, K. N. Kudin, V. N. Staroverov, R. Kobayashi, J. Normand, K. Raghavachari, A. Rendell, J. C. Burant, S. S. Iyengar, J. Tomasi, M. Cossi, N. Rega, J. M. Millam, M. Klene, J. E. Knox, J. B. Cross, V. Bakken, C. Adamo, J. Jaramillo, R. Gomperts, R. E. Stratmann, O. Yazyev, A. J. Austin, R. Cammi, C. Pomelli, J. W. Ochterski, R. L. Martin, K. Morokuma, V. G. Zakrzewski, G. A. Voth, P. Salvador, J. J. Dannenberg, S. Dapprich, A. D. Daniels, Ö. Farkas, J. B. Foresman, J. V. Ortiz, J. Cioslowski, D. J. Fox, Gaussian 09. *Gaussian, Inc.: Wallingford,CT, USA,*, **2009**.

[12] T. Lu, F. Chen, Multiwfn: A multifunctional wavefunction analyzer. *J. Comput. Chem.*,

2012. *33*, 580-592.

[13] P. Li, L. F. Song, K. M. Merz Jr, Parameterization of highly charged metal ions using the 12-6-4 LJ-type nonbonded model in explicit water. *J. Phys. Chem. B*, **2015**. *119*, 883-895.

[14]. H. J. Berendsen, J. v. Postma, W. F. Van Gunsteren, A. DiNola, J. R. Haak, Molecular dynamics with coupling to an external bath. *J. Chem. Phys.*, **1984**. *81*, 3684-3690.

[15]. U. Essmann, L. Perera, M. L. Berkowitz, T. Darden, H. Lee, L. G. Pedersen, A smooth particle mesh Ewald method. *J. Chem. Phys.*, **1995**. *103*, 8577-8593.

[16]. B. Hess, H. Bekker, H. J. Berendsen, J. G. Fraaije, LINCS: a linear constraint solver for molecular simulations. *J. Comput. Chem.*, **1997**. *18*, 1463-1472.

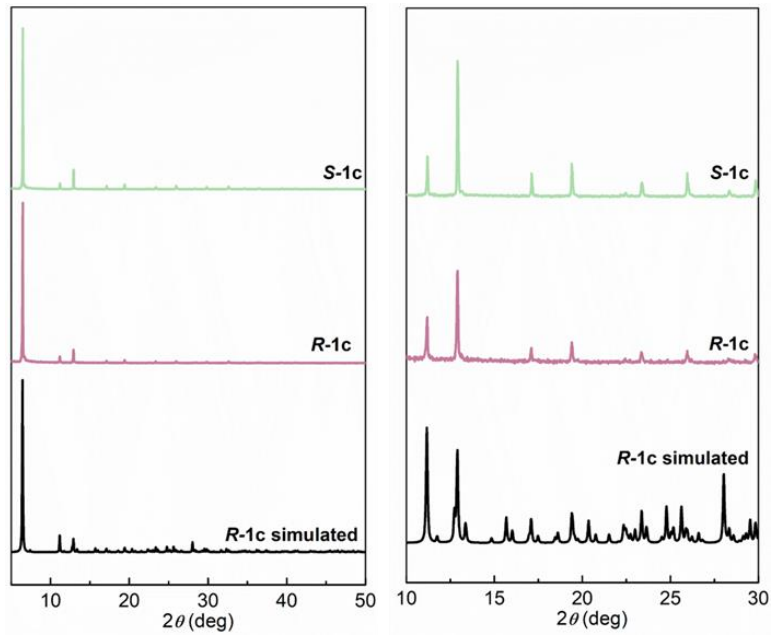

Figure S1. PXRD patterns of compounds ***R*-1c** and ***S*-1c**. The pattern simulated from the single crystal data of ***R*-1c** is given for comparison.

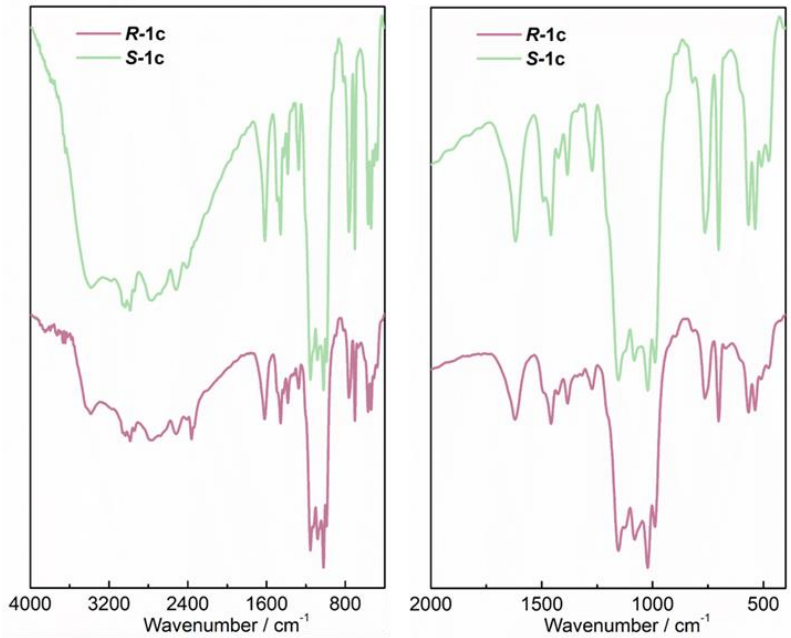

Figure S2. The IR spectra for compounds ***R*-1c** and ***S*-1c**.

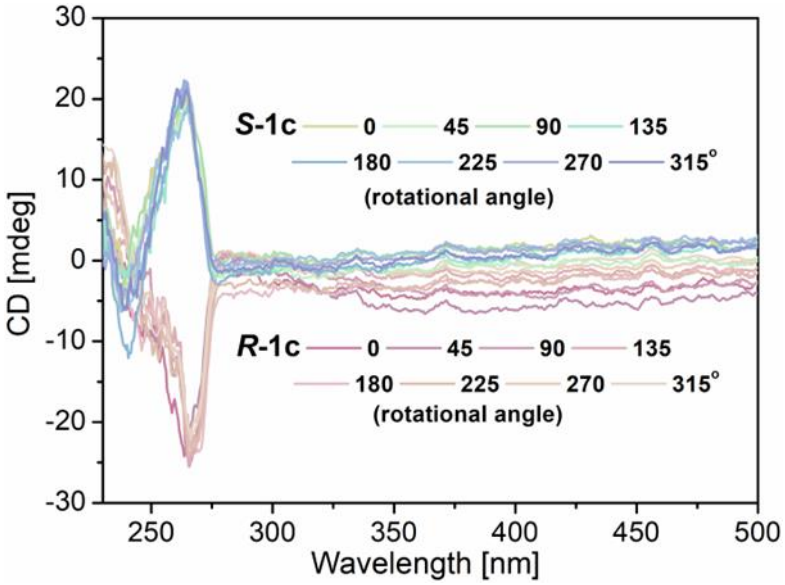

Figure S3. The angle dependence CD spectra of compounds ***R*-1c** and ***S*-1c.**

Table S1. Crystal data and structure refinements for ***R*-1c**.

Compounds	***R*-1c**
Formula	$C_{27}H_{39}N_3O_9P_3Dy\cdot H_2O$
M	823.04
Crystal system	Hexagonal
Space group	$P6_5$
T (K)	296
a (Å)	15.836(1)
b (Å)	15.836(1)
c (Å)	24.165(2)
α (°)	90
β (°)	90
γ (°)	120
V (Å^3)	5248.4(6)
D_c (g cm^{-3})	1.562
μ (mm^{-1})	2.326
F(000)	2490
R_{int}	0.0615
R_1, wR_2 [$I>2\sigma(I)$]	0.0615, 0.1682
GoF on F^2	1.017
Flack parameter	0.009(5)
CCDC number	2086980

$R_1 = \Sigma||F_o| - |F_c||/\Sigma|F_o|$, $wR_2 = [\Sigma w(F_o^2 - F_c^2)^2/\Sigma w(F_o^2)^2]^{1/2}$

Table S2. Selected bond lengths [Å] and angles [°] for ***R*-1c**.

Dy1-O1	2.418(7)	P1-O2	1.504(7)
Dy1-O2	2.488(7)	P1-O3	1.484(9)
Dy1-O4	2.372(7)	P2-O4	1.526(8)
Dy1-O5	2.647(7)	P2-O5	1.549(8)
Dy1-O7	2.298(9)	P2-O6	1.488(10)
Dy1-O5A	2.319(8)	P3-O7	1.528(8)
Dy1-O8A	2.261(9)	P3-O8	1.488(8)
Dy1-O2B	2.351(8)	P3-O9	1.385(10)
P1-O1	1.513(7)		
O1-Dy1-O2	58.5(2)	O4-Dy1-O7	95.1(3)
O1A-Dy1-O4	80.5(2)	O4-Dy1-O5A	77.1(3)
O1A-Dy1-O5	83.9(2)	O4-Dy1-O8A	163.1(3)
O1A-Dy1-O7	154.0(3)	O4-Dy1-O2B	119.8(3)
O1-Dy1-O5A	120.3(3)	O5-Dy1-O7	72.4(3)
O1-Dy1-O8A	102.6(3)	O5-Dy1-O5A	124.7(2)
O1-Dy1-O2B	75.9(3)	O5-Dy1-O8A	138.9(2)
O2-Dy1-O4	93.4(2)	O5-Dy1-O2B	65.3(2)
O2-Dy1-O5	136.9(2)	O7-Dy1-O5A	83.0(3)
O2-Dy1-O7	147.5(3)	O7-Dy1-O8A	89.1(3)
O2-Dy1-O5A	68.5(3)	O7-Dy1-O2B	84.4(3)
O2-Dy1-O8A	74.8(3)	O5A-Dy1-O8A	87.3(3)
O2-Dy1-O2B	117.9(2)	O5A-Dy1-O2B	159.9(3)
O4-Dy1-O5	57.6(2)	O8A-Dy1-O2B	76.9(3)

Symmetry transformations used to generate equivalent atoms: A: x-y, x, -1/6+z; B: y, -x+y, 1/6+z.

Table S3. Hydrogen bonds among phosphonate groups, -NH_2- groups, -CH_2- groups, phenyl groups, water molecules in ***R*-1c**.

D-H···A	*d*(D-H) (Å)	*d*(H···A) (Å)	*d*(D···A) (Å)	∠ DHA (°)
C22—H22C···O9^{ii}	0.96	2.67	3.388(16)	132
C21—H21···O1W	0.98	2.39	3.00(2)	120
N3—H3D···O9^{ii}	0.97	1.86	2.817(13)	167
N3—H3E···O1W	0.97	2.13	2.84(2)	129
O1W—H1WB···O7	0.85	2.39	3.037 (19)	134
O1W—H1WA···O6	0.85	1.98	2.82 (3)	168
N2—H2B···O4^{ii}	0.97	1.77	2.720 (11)	167
N2—H2A···O1	0.97	1.82	2.770 (11)	166
N1—H1D···O3^{ii}	0.97	1.71	2.675 (11)	172
N1—H1C···O9^{i}	0.97	2.10	3.033 (13)	160
N1—H1C···O8^{i}	0.97	2.56	3.342 (12)	138
C3—H3A···O3^{ii}	0.96	2.62	3.319 (14)	130

Symmetry transformations used to generate equivalent atoms: i: x-y, x, -1/6+z; ii: y, -x+y, 1/6+z.

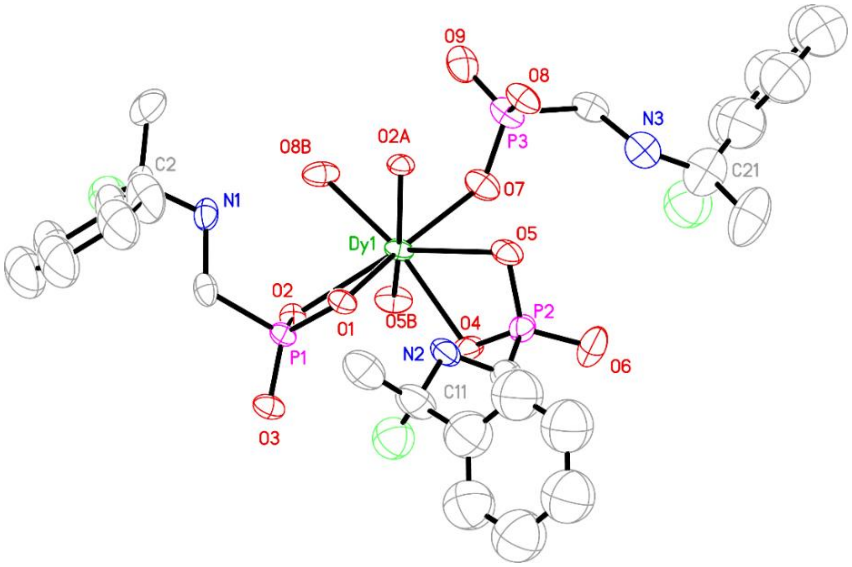

Figure S4. ORTEP view of ***R*-1c** with 30% thermal ellipsoids. All H atoms except those attached to the chiral carbon centers are omitted for clarity. All C atoms except the chiral centers are not labeled.

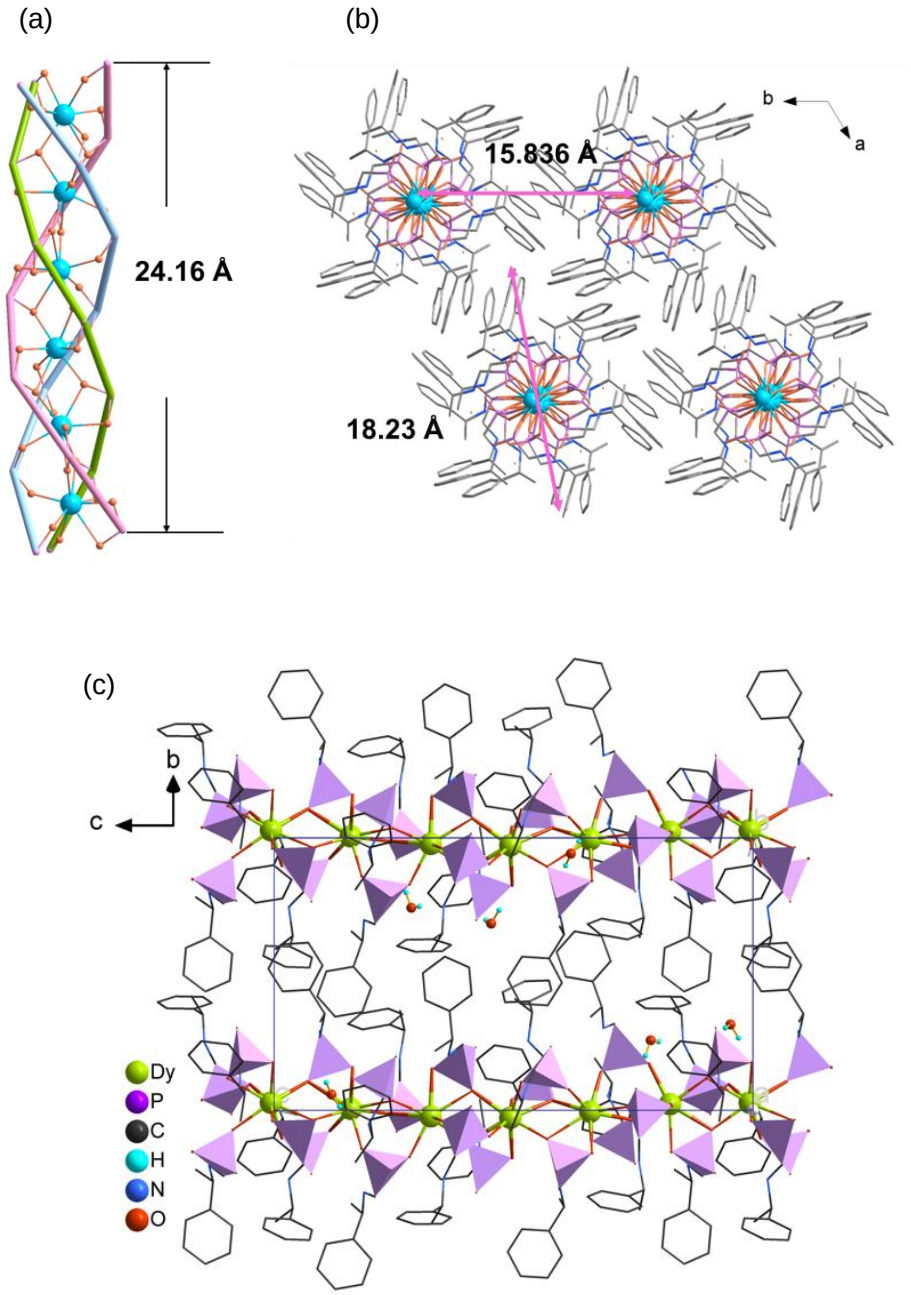

Figure S5. (a) Single inorganic chain in ***R*-1c**. (b) Packing diagram of ***R*-1c** viewed along the *c*-axis. (c) Packing diagram of ***R*-1c** viewed along the *a*-axis.

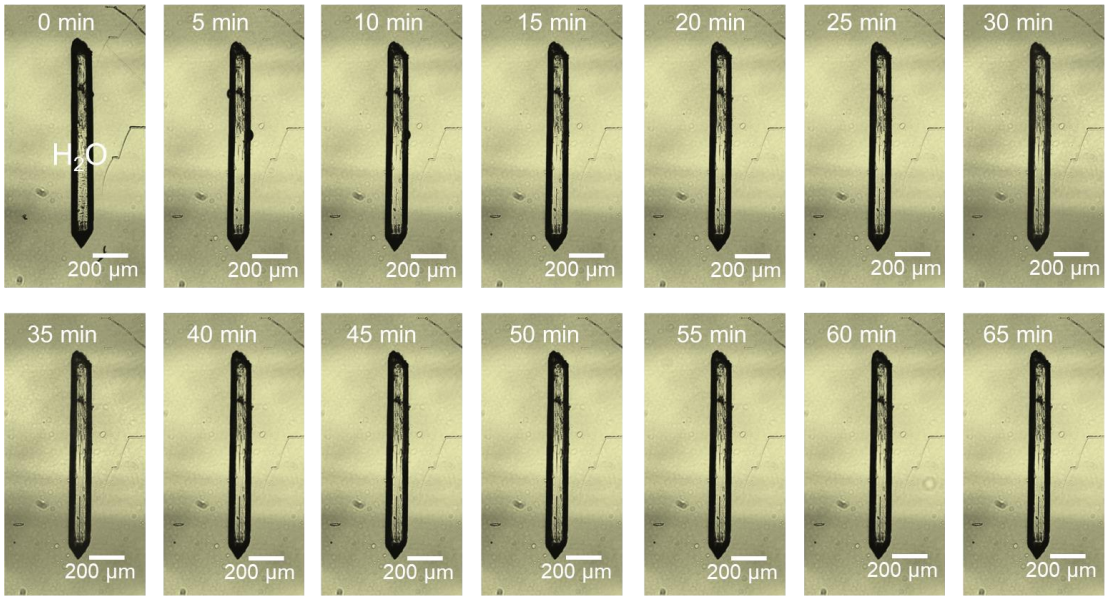

Figure S6. Morphology changes of ***R*-1c** crystal over time after immersing in water.

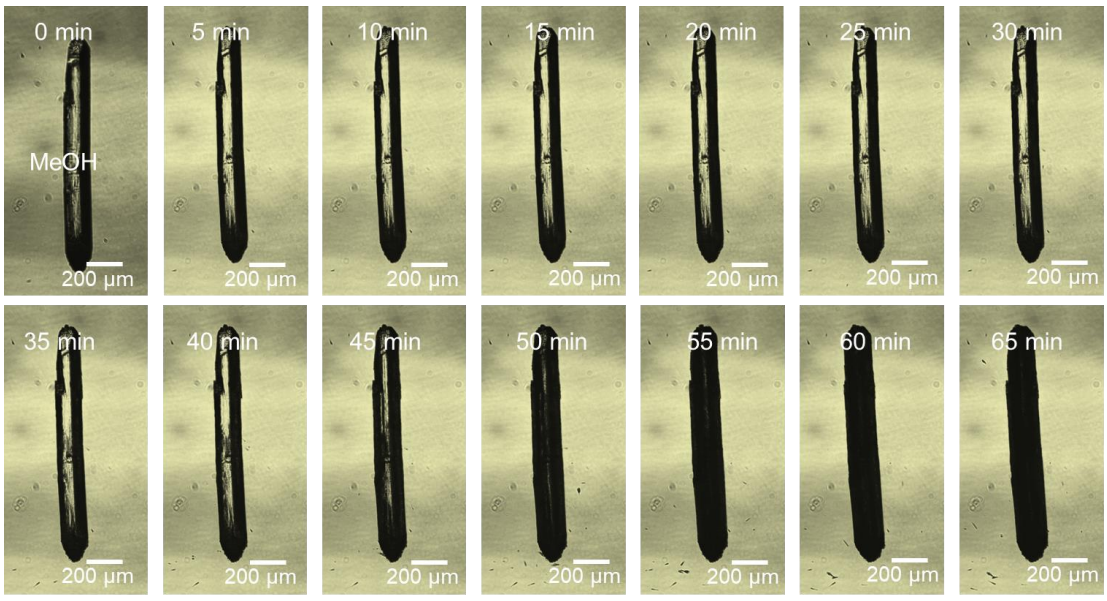

Figure S7. Morphology changes of ***R*-1c** crystal over time after immersing in methanol.

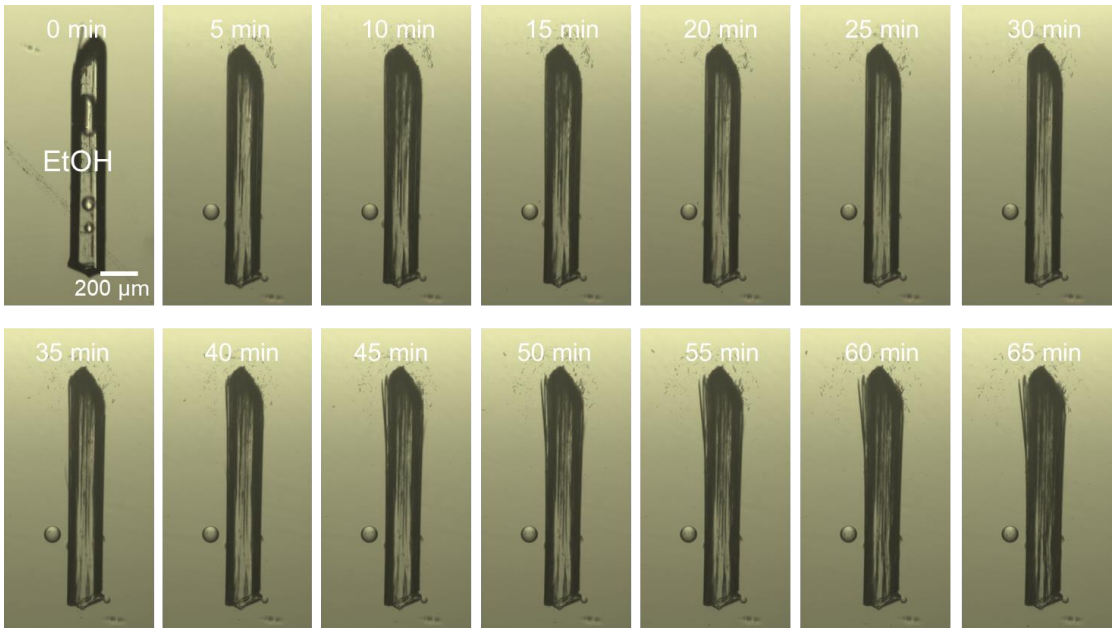

Figure S8. Morphology changes of ***R*-1c** crystal overe time after immersing in ethanol.

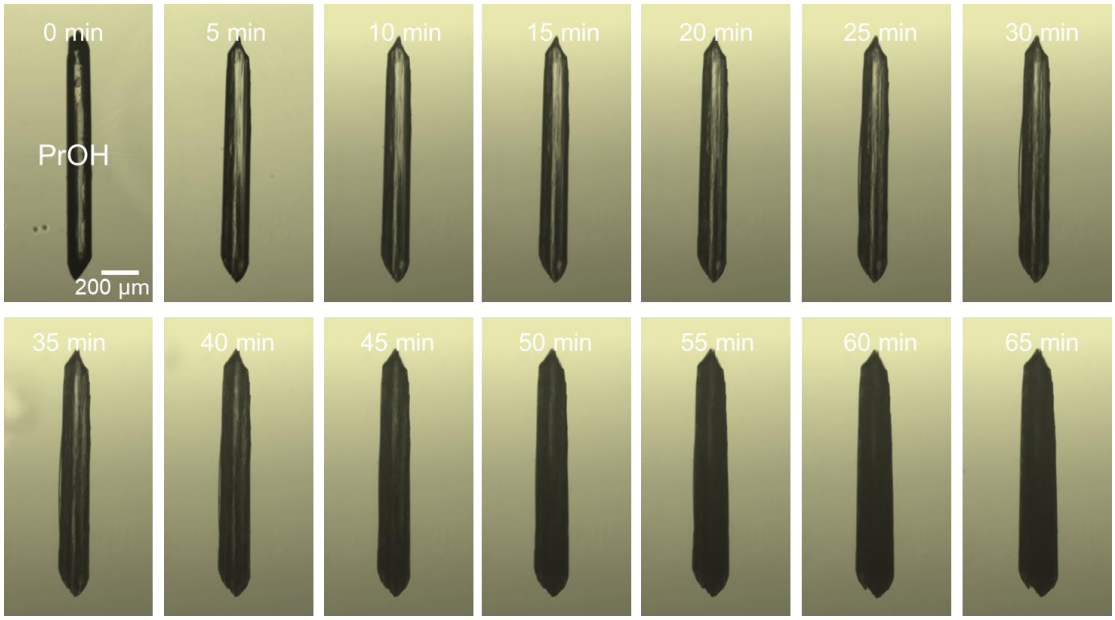

Figure S9. Morphology changes of ***R*-1c** crystal over time after immersing in n-propanol.

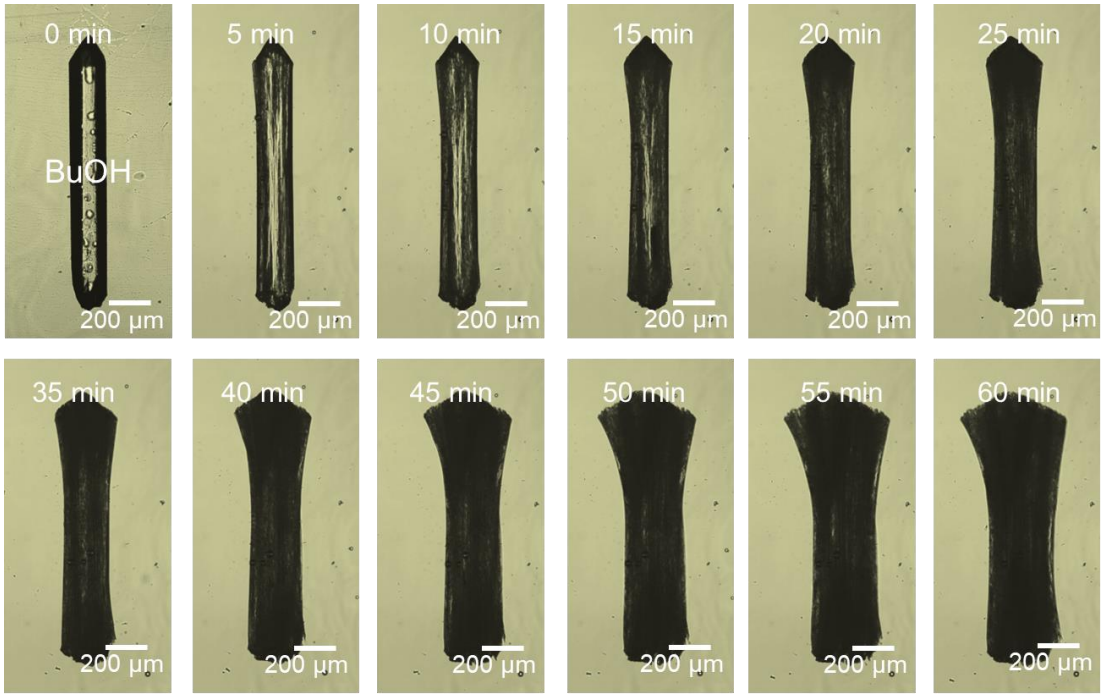

Figure S10. Morphology changes of ***R*-1c** crystal over time after immersing in n-butanol.

Table S4. The expansion width before (d_0) and after (d_t) the immersion. The expansion rate is also estimated by the equation [$(d_t-d_0)/d_0$].

Solvent	**Initial Diameter (d_0, μm)**	**Final Diameter (d_t, μm)**	**$(d_t-d_0)/d_0$**
CH_3OH	168	217	29%
C_2H_5OH	189	247	31%
C_3H_7OH	150	209	39%
C_4H_9OH	181	407	125%

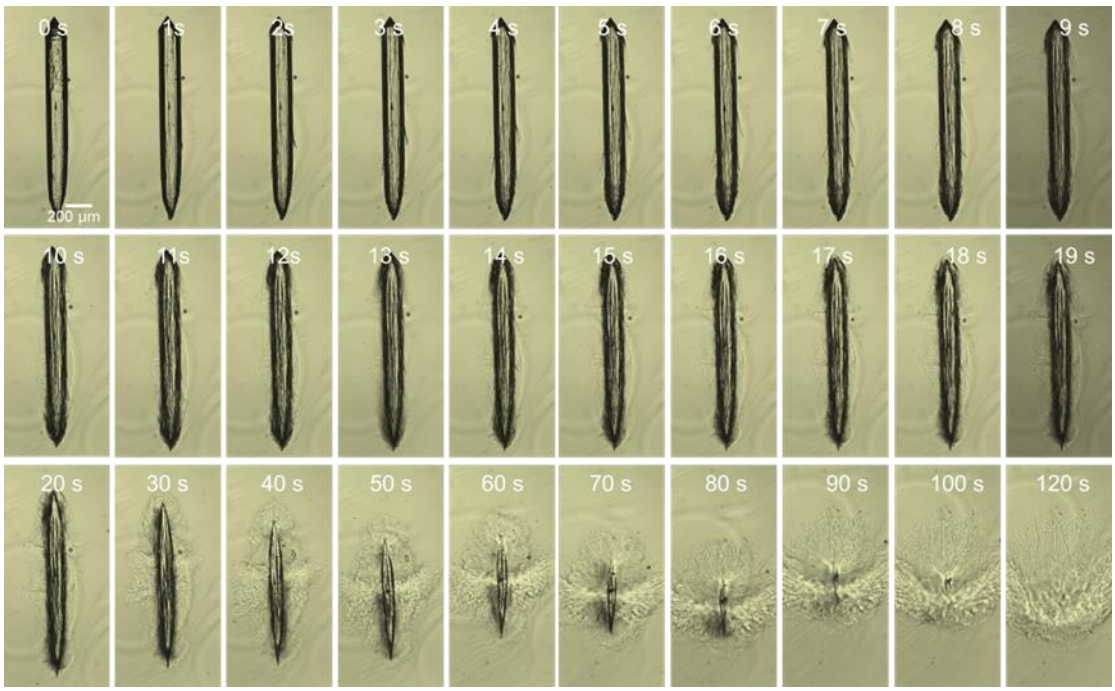

Figure S11. Morphology changes of ***R*-1c** crystal over time after immersing in CH_2Cl_2.

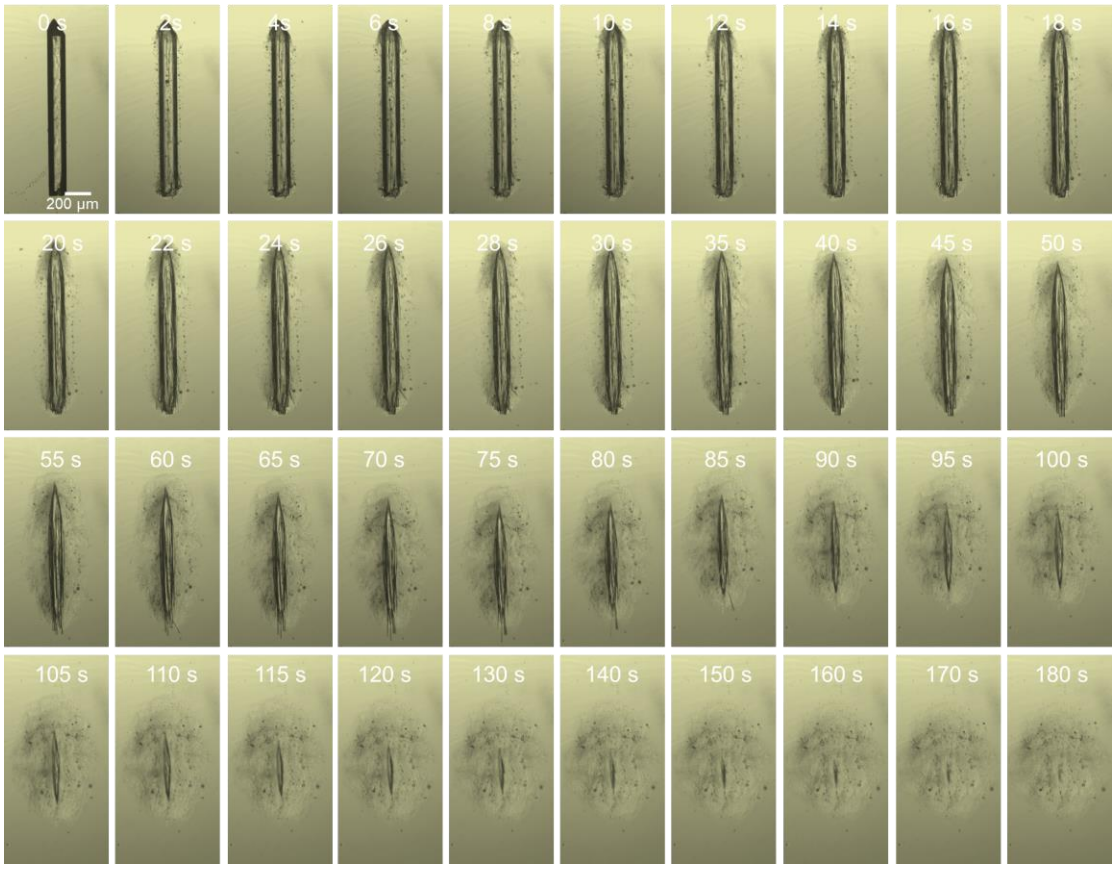

Figure S12. Morphology changes of ***R*-1c** crystal over time after immersing in $CHCl_3$.

Figure S13. Morphology changes of ***R*-1c** crystal over time after immersing in CH_2Br_2.

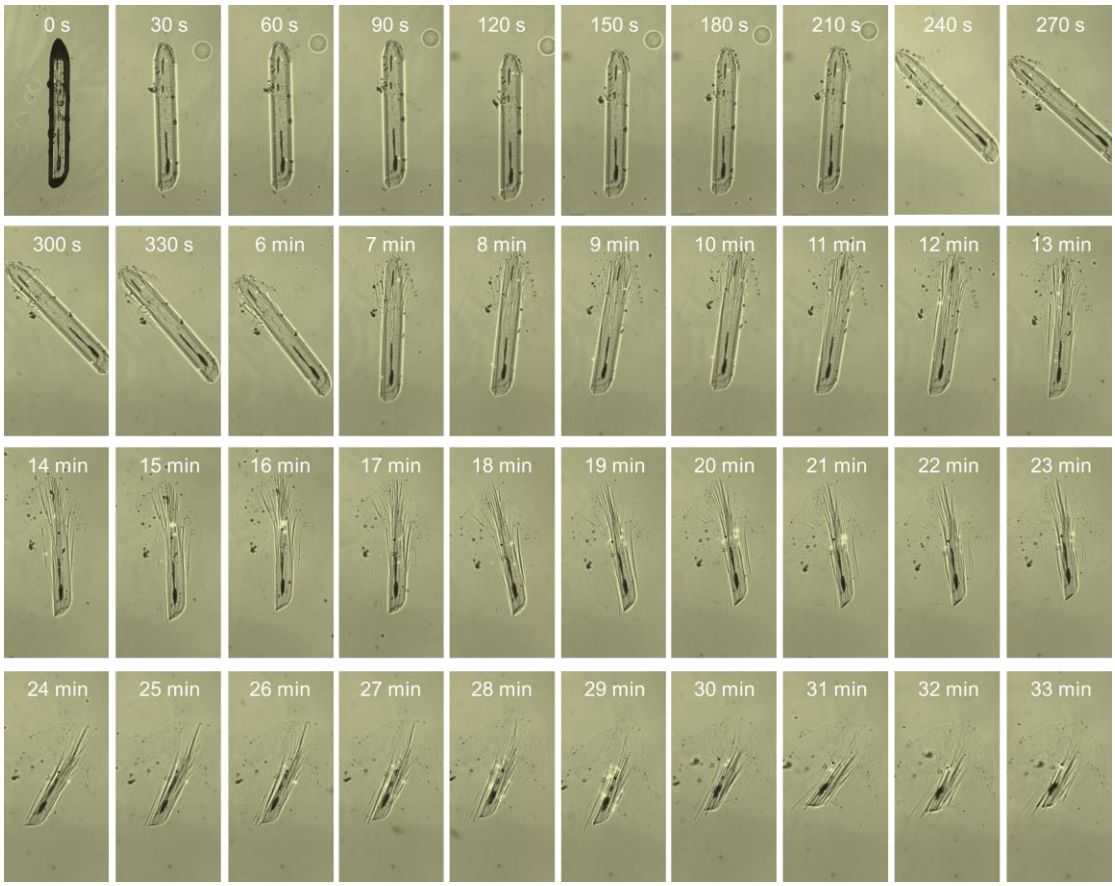

Figure S14. Morphology changes of ***R*-1c** crystal over time after immersing in $CHBr_3$.

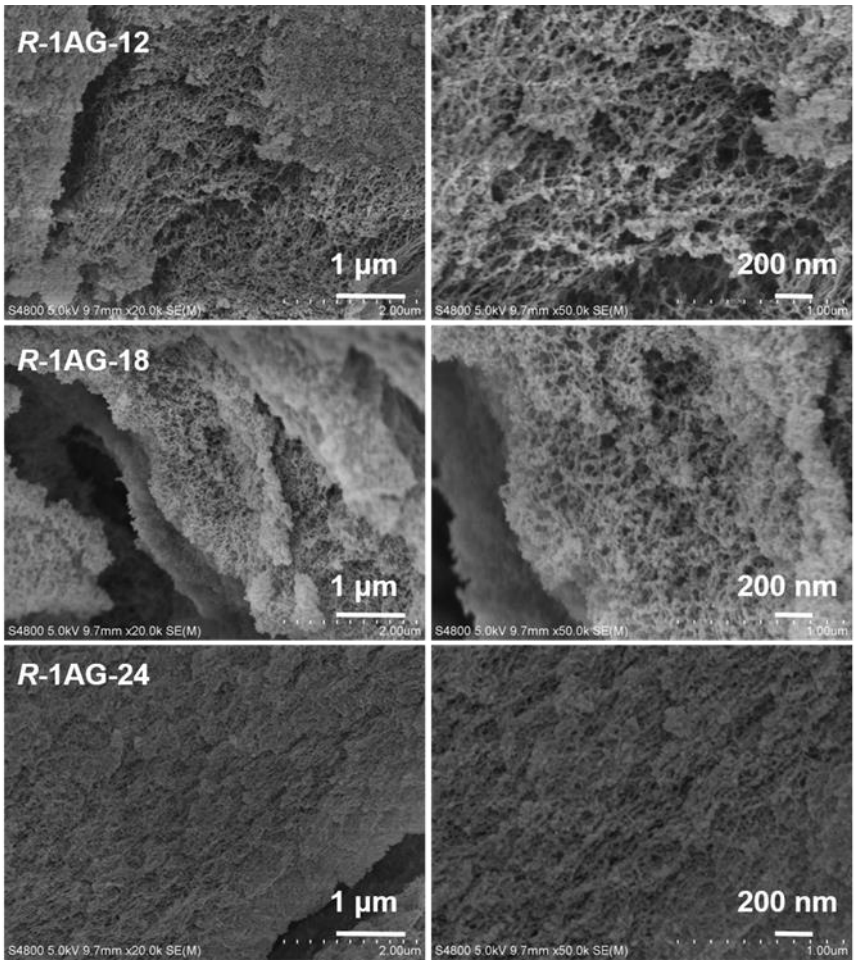

Figure S15. The SEM images for the aerogels ***R*-1AG-12**, ***R*-1AG-18** and ***R*-1AG-24**.

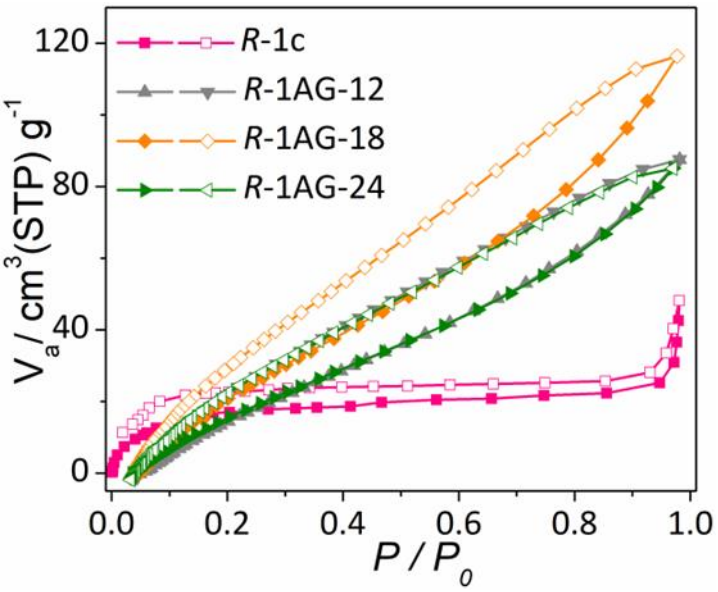

Figure S16. Methanol sorption isotherms of ***R*-1c**, ***R*-1AG-12**, ***R*-1AG-18**, and ***R*-1AG-24** at 298 K.

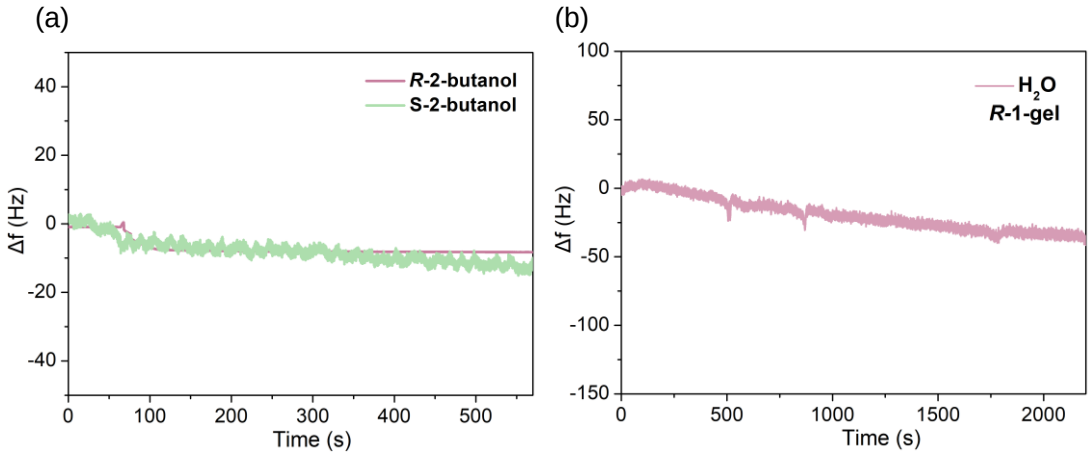

Figure S17. (a) The *Δf* versus time curves of *R*- and *S*-2-butanol adsorbed on blank QCM Au electrode. (b) The *Δf* versus time curve of pure water adsorbed on QCM Au electrode covered with ***R*-1AG-18**.

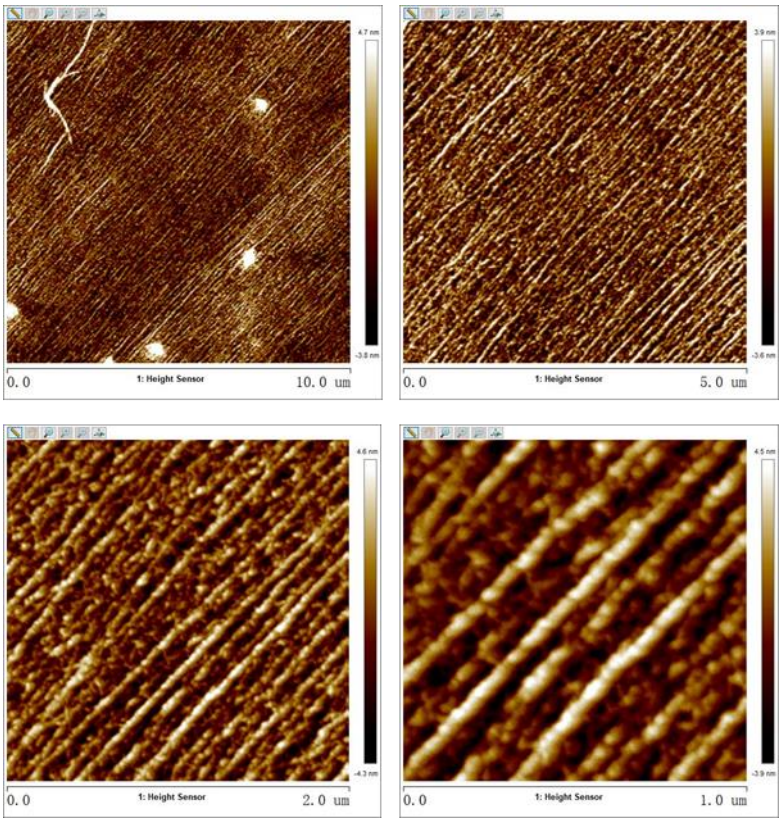

Figure S18. AFM images of ***R*-1c** after dispersing in $CHCl_3$ for 2 min (concentration 0.12 mmol/L).

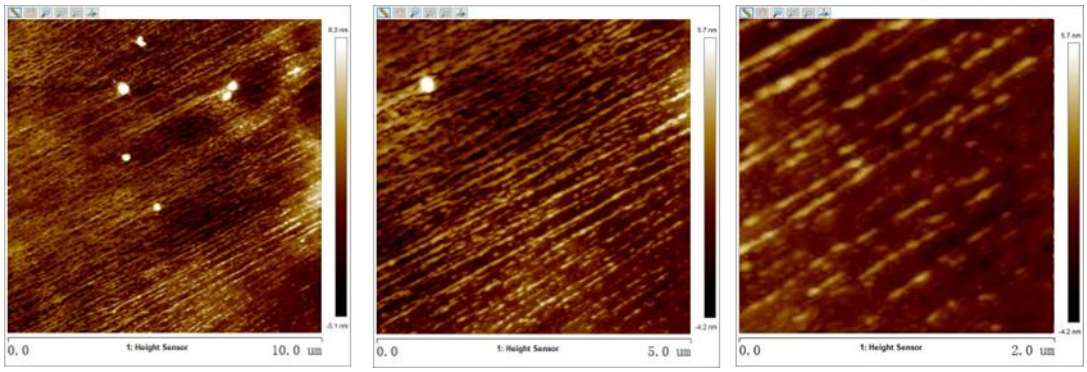

Figure S19. AFM images of ***R*-1c** after dispersing in $CHCl_3$ for 5 min (concentration 0.12 mmol/L).

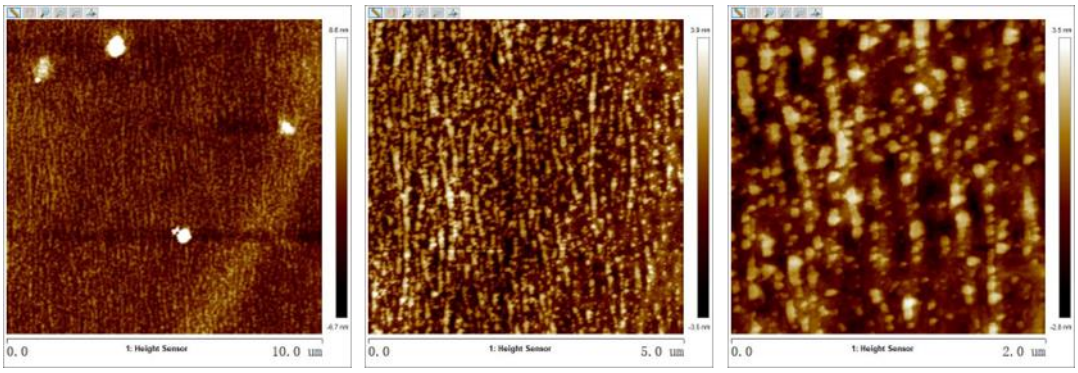

Figure S20. AFM images of ***R*-1c** after dispersing in $CHCl_3$ for 10 min (concentration 0.12 mmol/L).

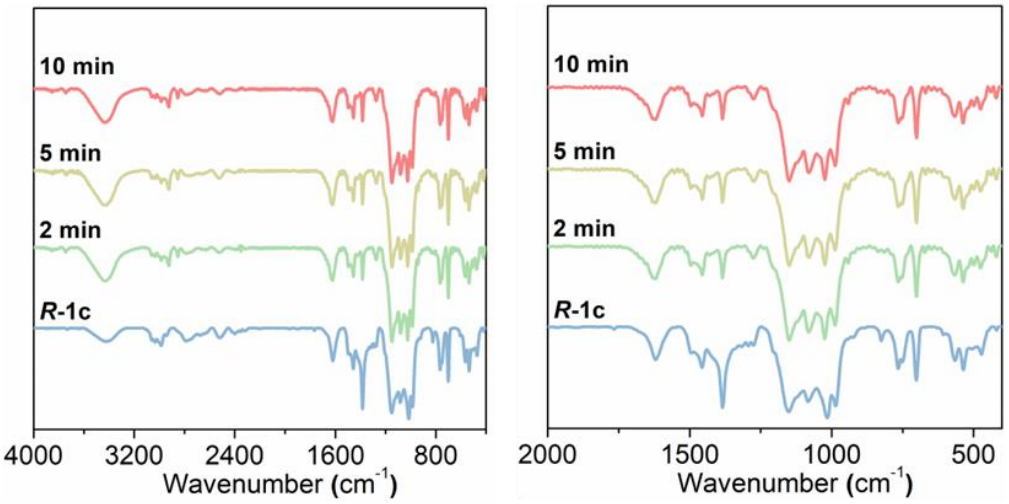

Figure S21. The IR spectra of the solid residues obtained by solvent evaporation from dispersions of ***R*-1c** in $CHCl_3$ for 5, 10 and 20 min (concentration 0.12 mmol/L).

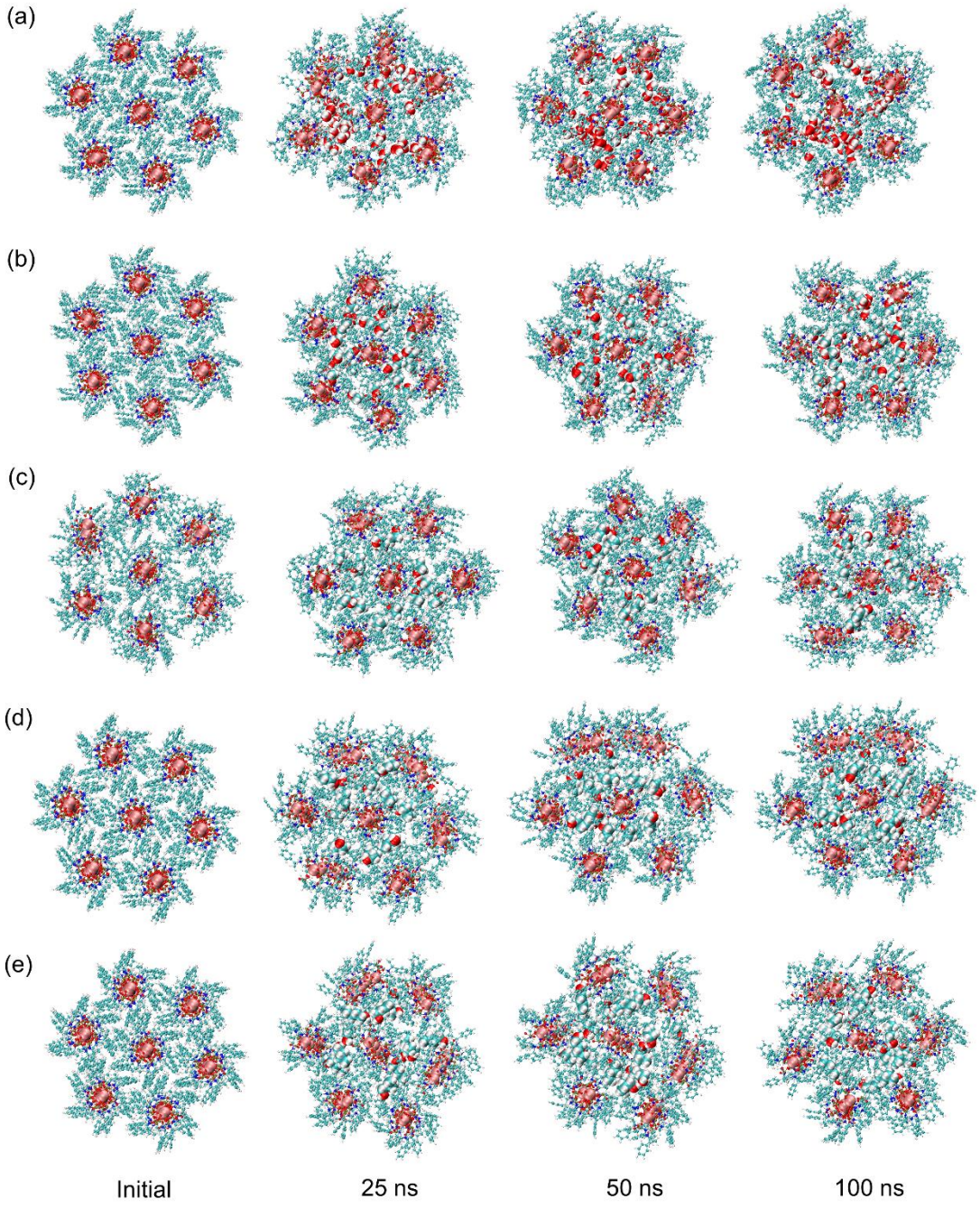

Figure S22. Snapshots depicting the time evolution of ***R*-1c** crystals in water (a), methanol (b), ethanol (c), n-propanol (d), and n-butanol (e).

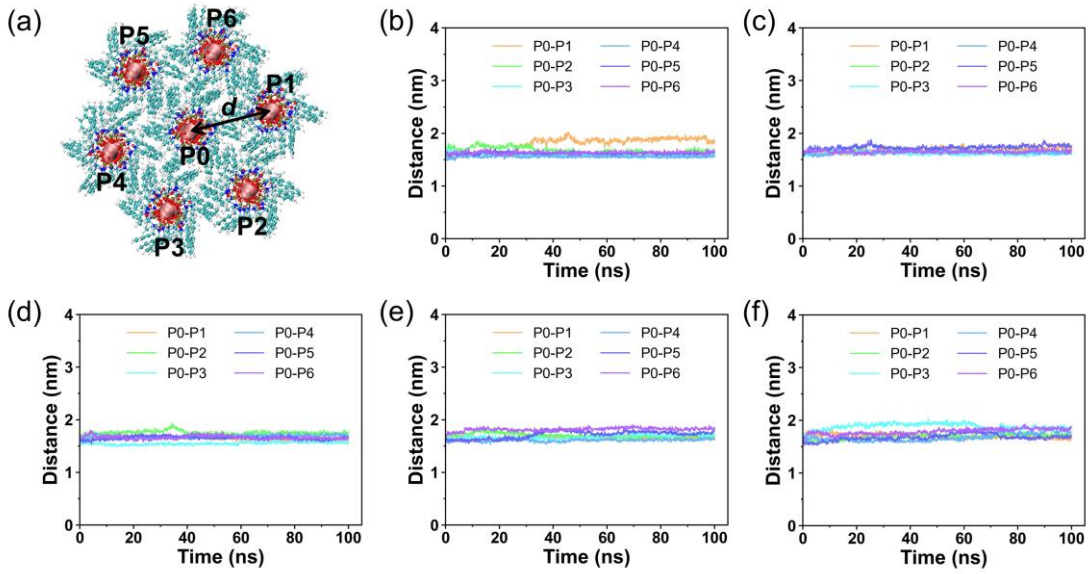

Figure S23. (a) Schematic diagram of the distance between chains in ***R*-1c** crystal. Distances between the peripheral chains and the central chain in ***R*-1c** crystals in water (b), methanol (c), ethanol (d), n-propanol (e), and n-butanol (f).

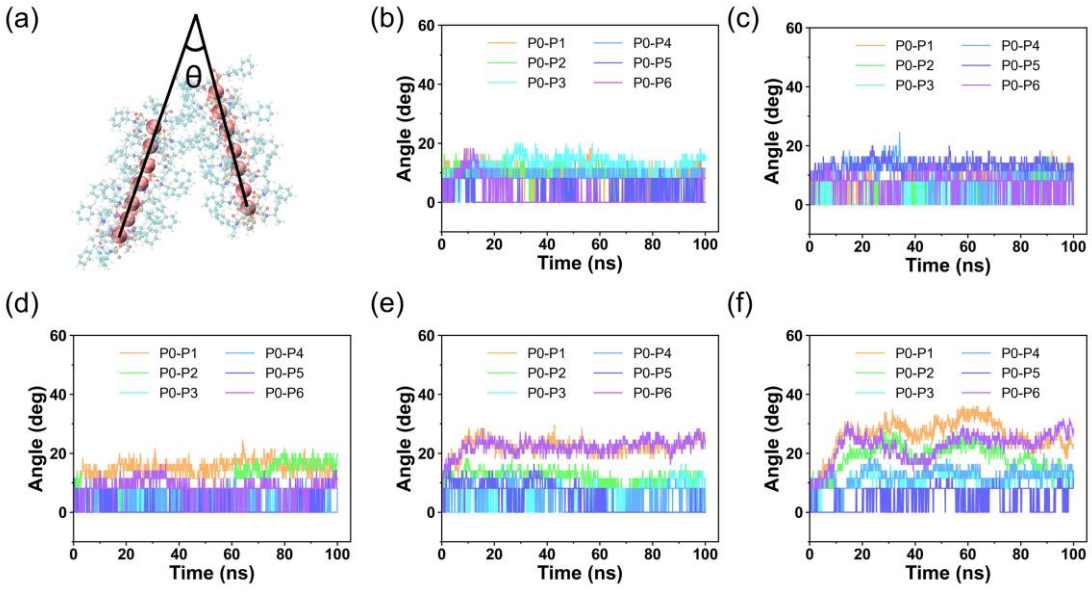

Figure S24. (a) Schematic diagram of the angle between chains in ***R*-1c** crystal. Angles between the peripheral chains and the central chain in R-1 crystals in water (b), methanol (c), ethanol (d), n-propanol (e), and n-butanol (f).

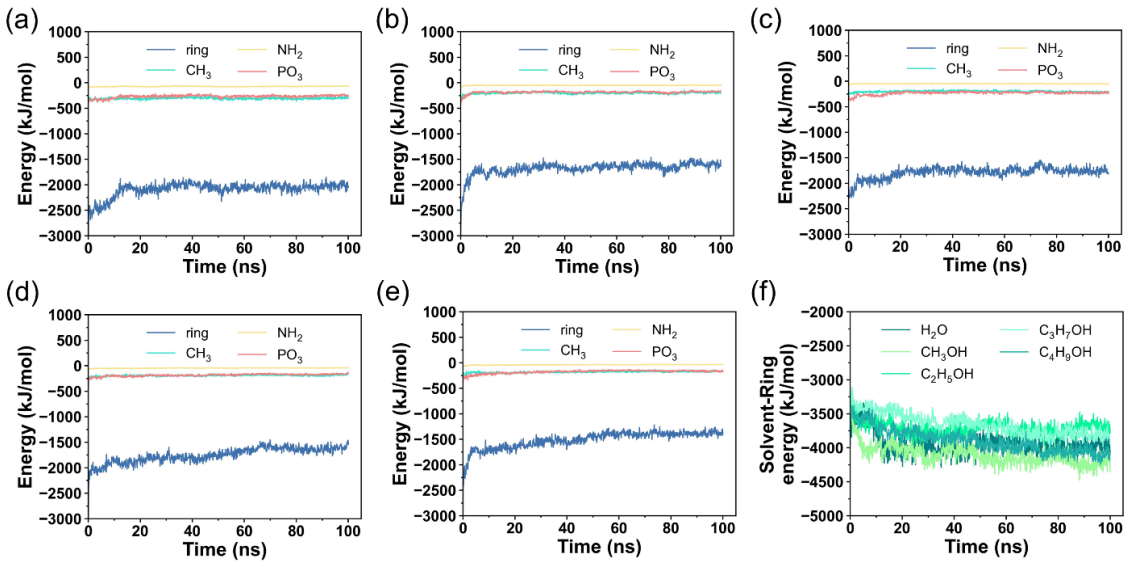

Figure S25. The interaction energy contributed by aromatic ring, -NH_2, -CH_3 and -PO_3 for maintaining ***R*-1c** crystal structures in water (a), methanol (b), ethanol (c), n-propanol (d), and n-butanol (e). (f) The interaction energy between solvent and aromatic rings of ***R*-1c**.

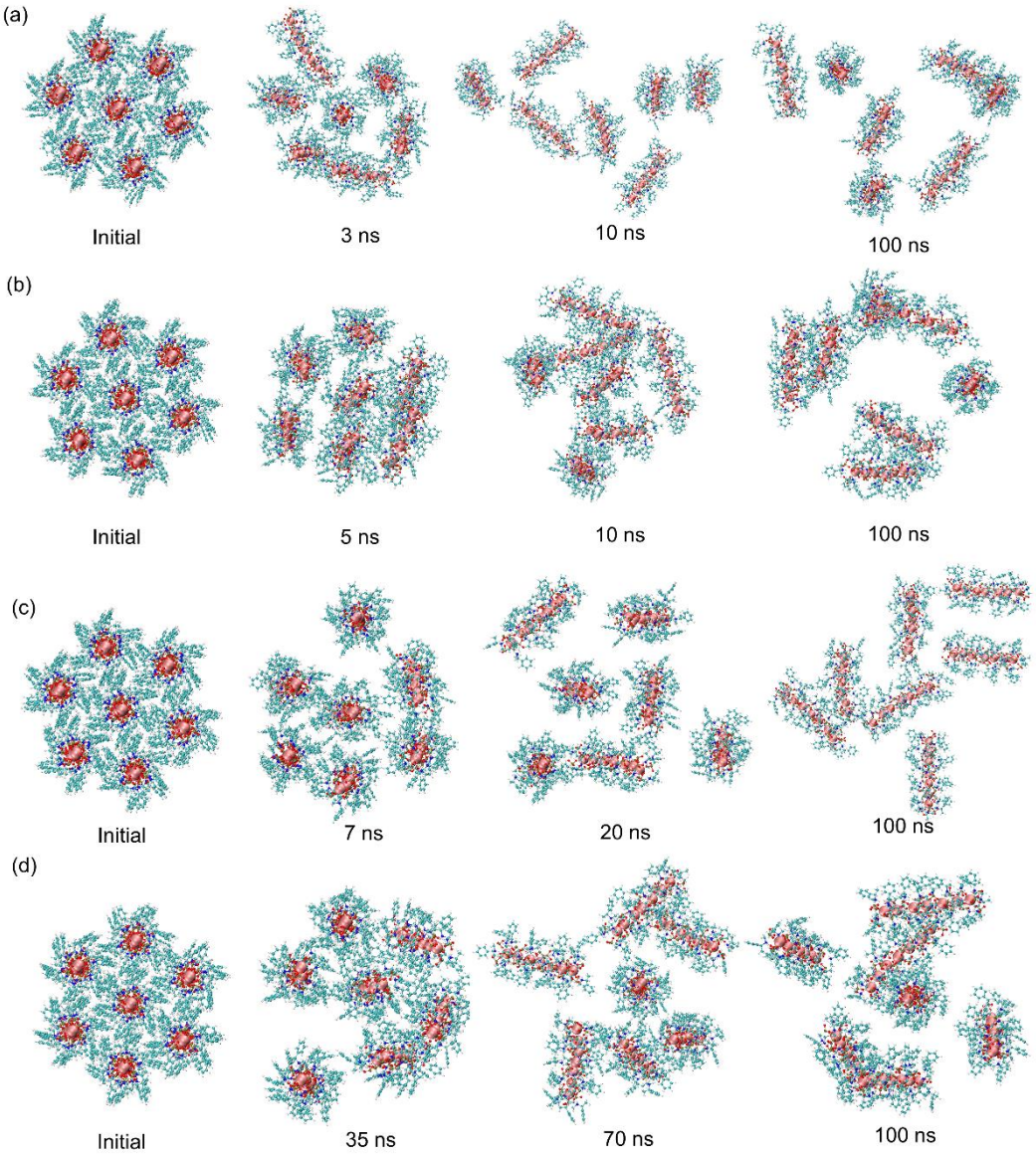

Figure S26. Snapshots depicting the time evolution of ***R*-1c** crystals in CH_2Cl_2 (a), $CHCl_3$ (b), CH_2Br_2 (c), $CHBr_3$ (d).

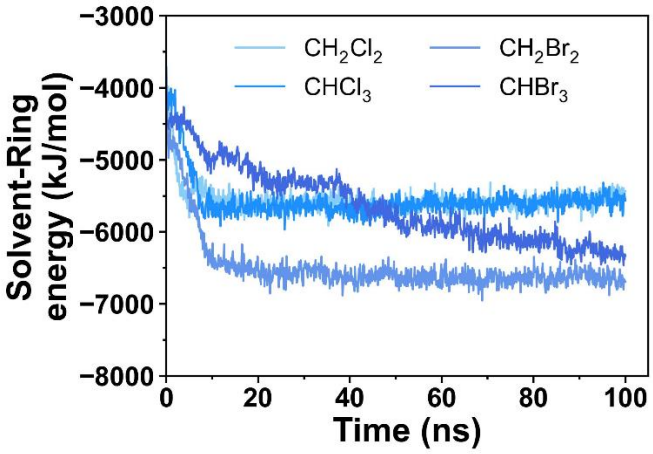

Figure S27. The interaction energy between solvent and aromatic rings of ***R*-1c**.

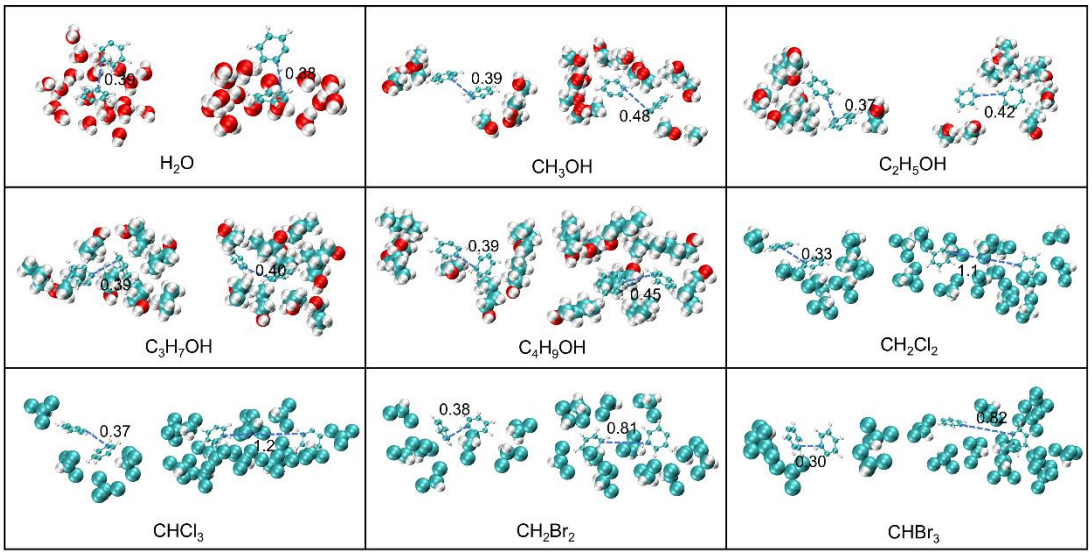

Figure S28. Typical snapshots of the local structures depicting the interchain ring-ring interaction is disrupted by the solvent molecules in halomethane solvents. In each subplot, the left side represents the initial structure of the simulation, while the right side corresponds to 100 ns for water and alkyl alcohol solvents, and the initial stage of stripping for halomethane solvents.

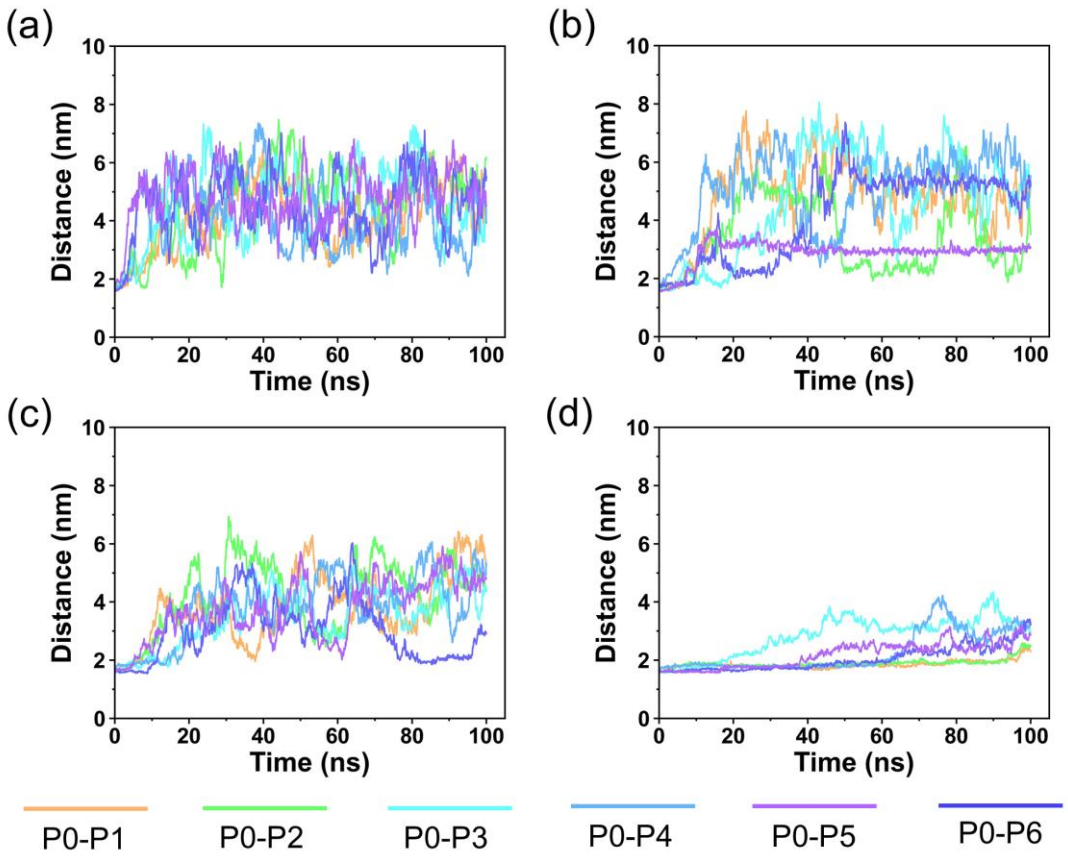

Figure S29. Distances between the peripheral chains and the central chain in ***R*-1c** crystals in CH_2Cl_2 (a), $CHCl_3$ (b), CH_2Br_2 (c), $CHBr_3$ (d).

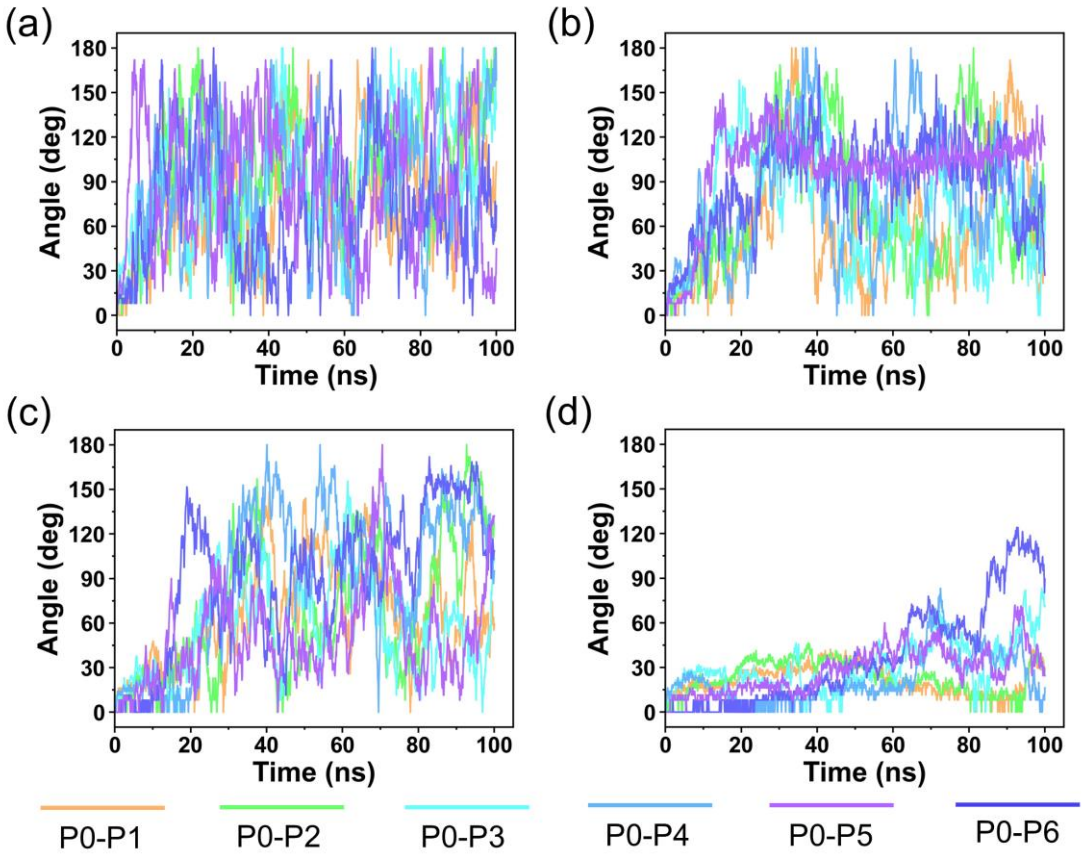

Figure S30. Angles between the peripheral chains and the central chain in ***R*-1c** crystals in CH_2Cl_2 (a), $CHCl_3$ (b), CH_2Br_2 (c), $CHBr_3$ (d). The chain is defined as stripped if the angle between it and the central chain is larger than 30.

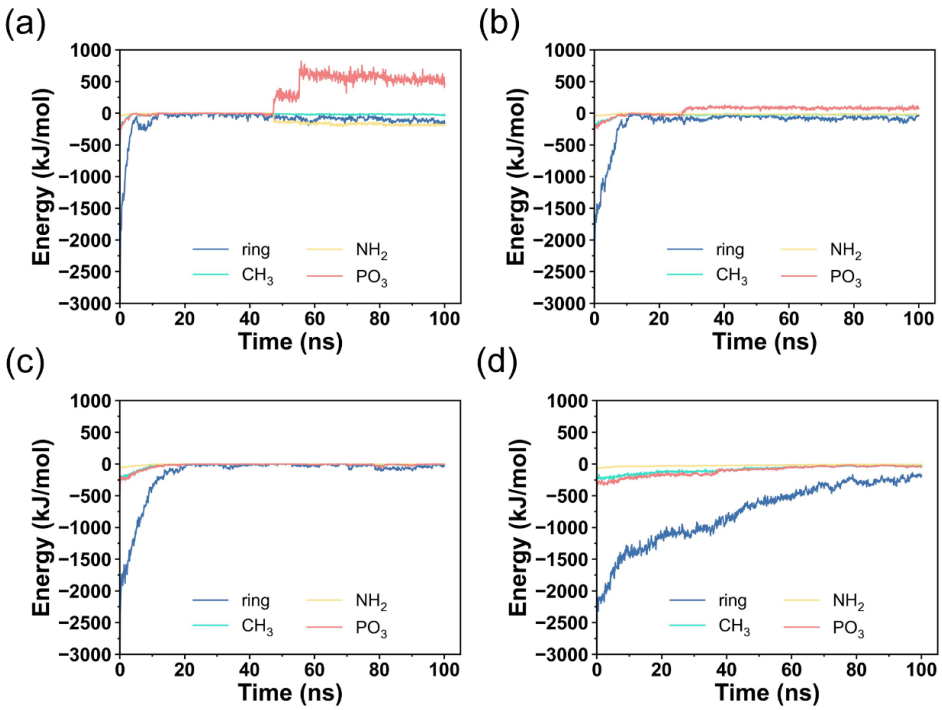

Figure S31. The interaction energy contributed by aromatic ring, -NH_2, -CH_3 and -PO_3 for maintaining ***R*-1c** crystal structures in CH_2Cl_2 (a), $CHCl_3$ (b), CH_2Br_2 (c), $CHBr_3$ (d).

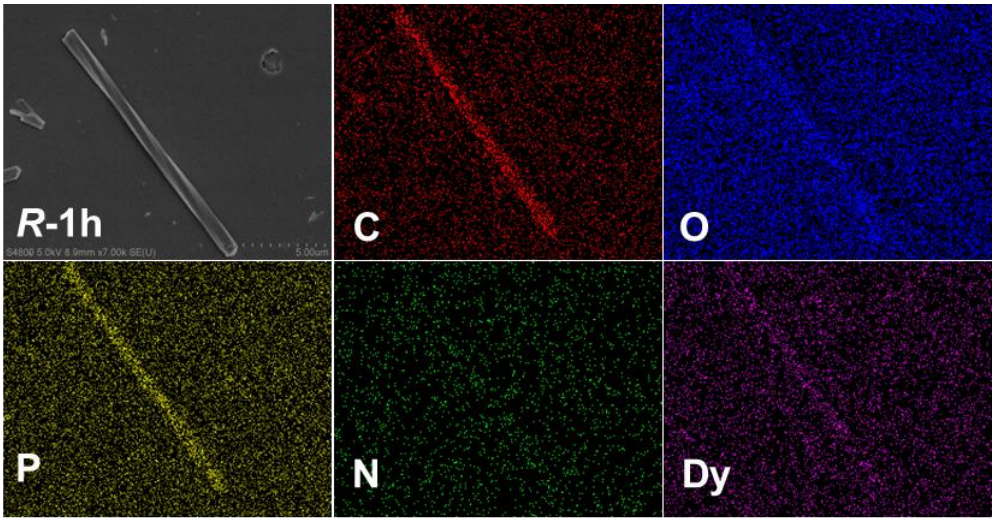

Figure S32. EDX elemental mapping of helices ***R*-1h**.

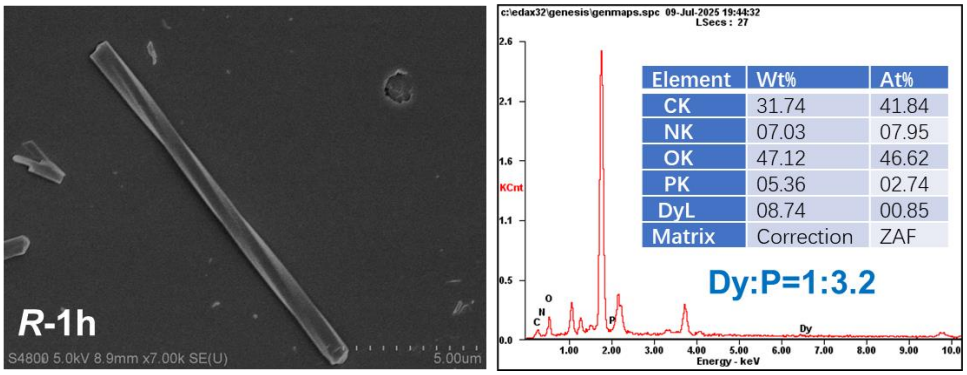

Figure S33. EDX spectra of helices ***R*-1h**.

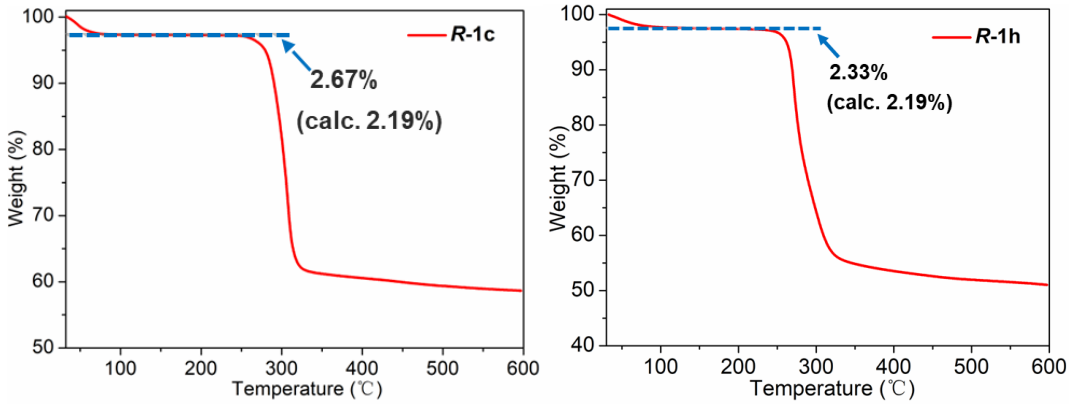

Figure S34. TGA curves of ***R*-1c** and ***R*-1h**. The weight losses in the temperature 30-110 °C agree well with the valued expected for the removal of one lattice water molecules.

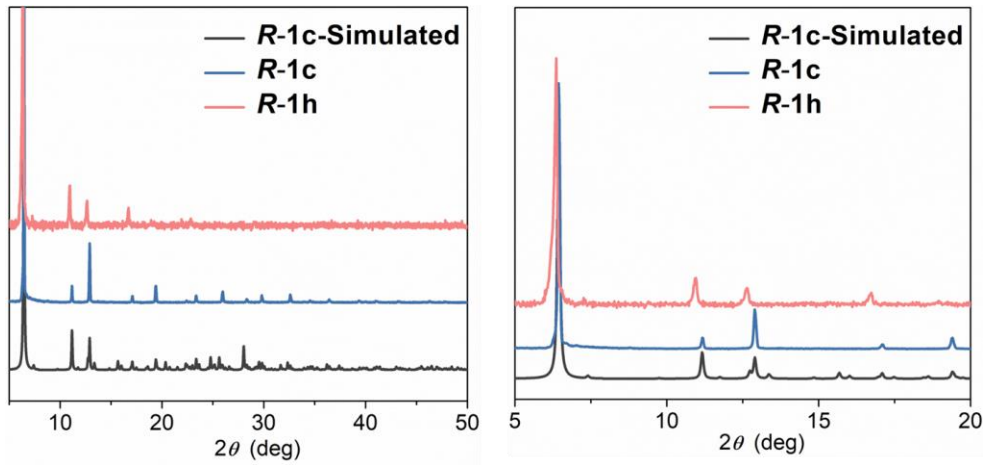

Figure S35. Powder XRD patterns of compounds ***R*-1c** and ***R*-1h**. The pattern simulated from the single crystal data of ***R*-1c** is given for comparison.

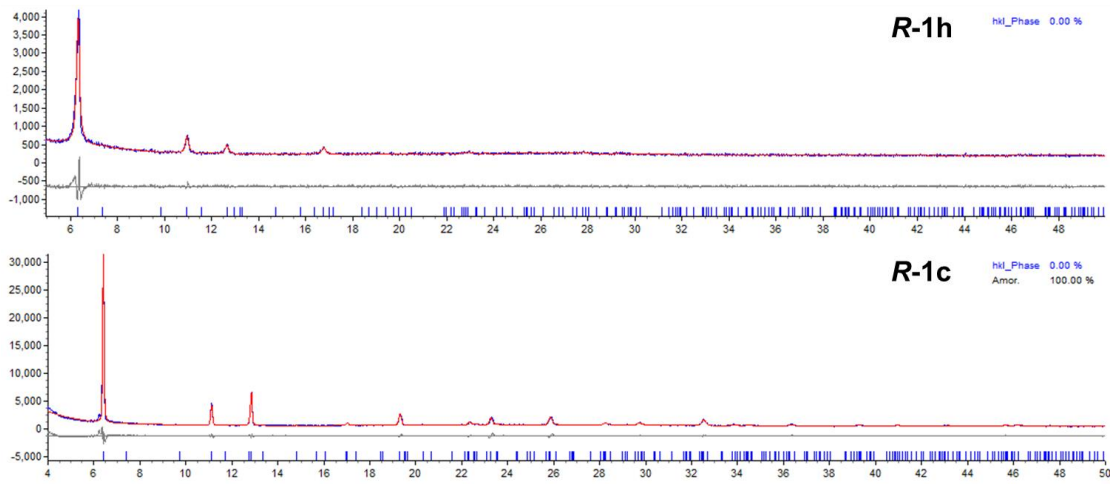

Figure S36. Pawley fit of the PXRD patterns of the powder samples of ***R*-1c** and ***R*-1h** using TOPAS 5.0 program.

Fitted cell parameters for ***R*-1h:** $P6_5$, a = 16.164 Å, c = 23.445 Å, V = 5304.8 Å^3 (Rwp = 7.44). For ***R*-1c:** $P6_5$, a = 15.915 Å, c = 24.069 Å, V = 5279.5 Å^3 (Rwp = 7.84).

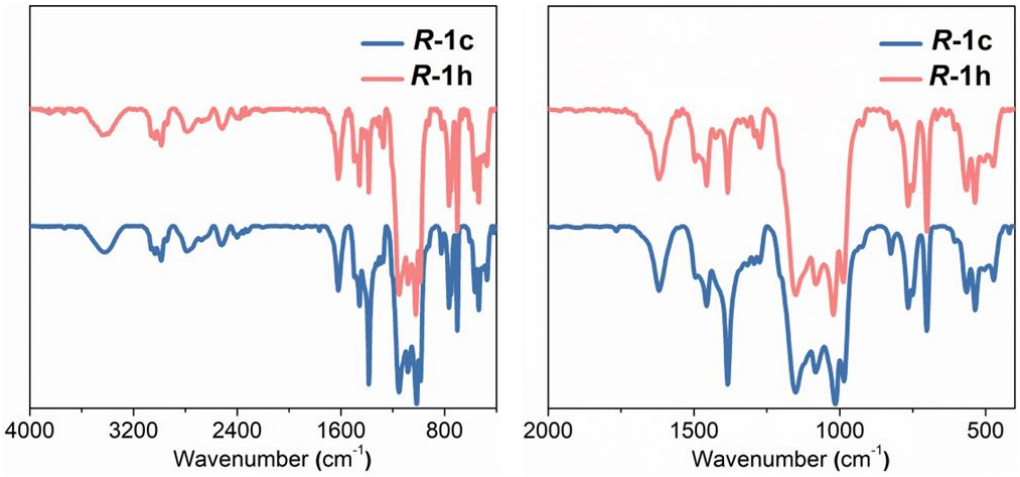

Figure S37. The IR spectra of compounds ***R*-1c** and ***R*-1h**.

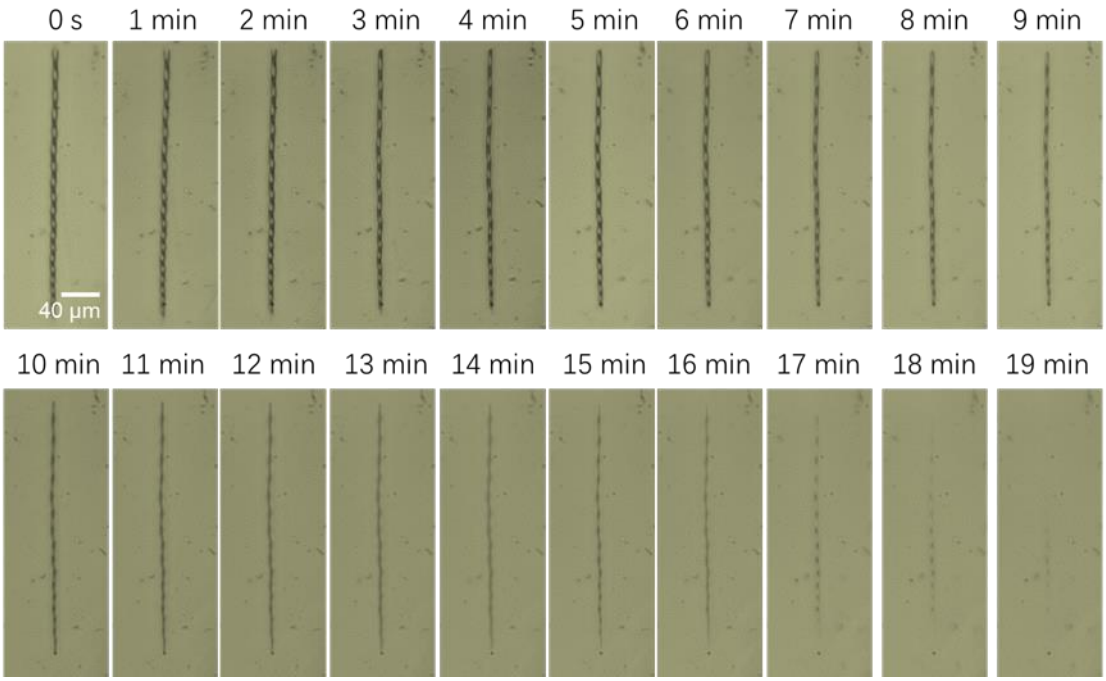

Figure S38. Morphology changes of ***R*-1h** helices immersed in CH_2Cl_2.

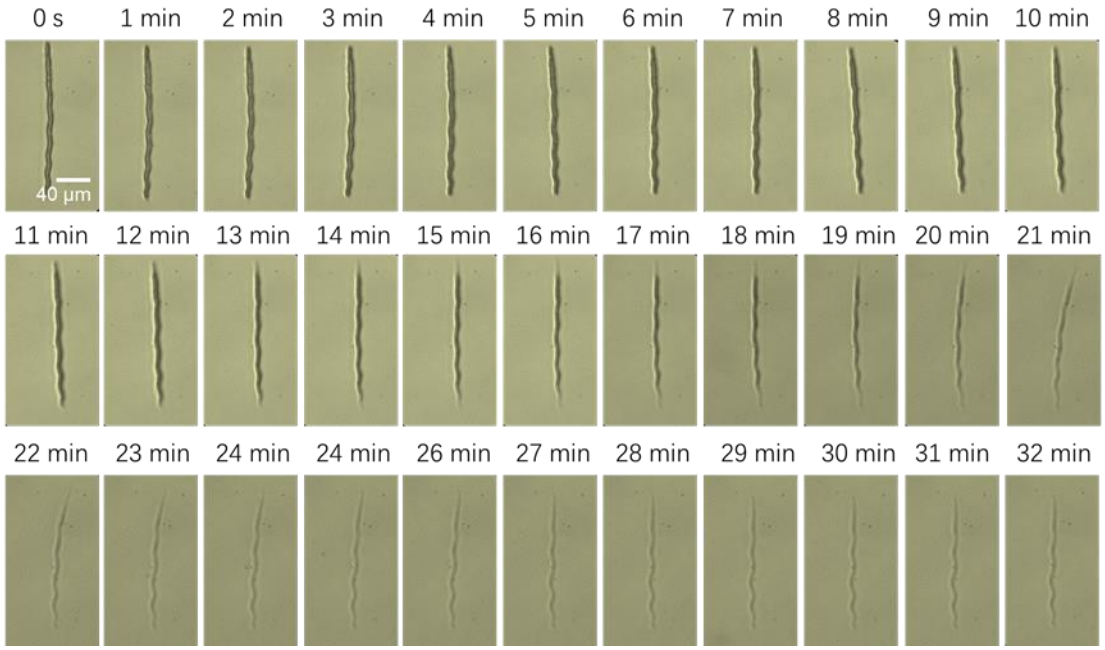

Figure S39. Morphology changes of ***R*-1h** helices immersed in $CHCl_3$.

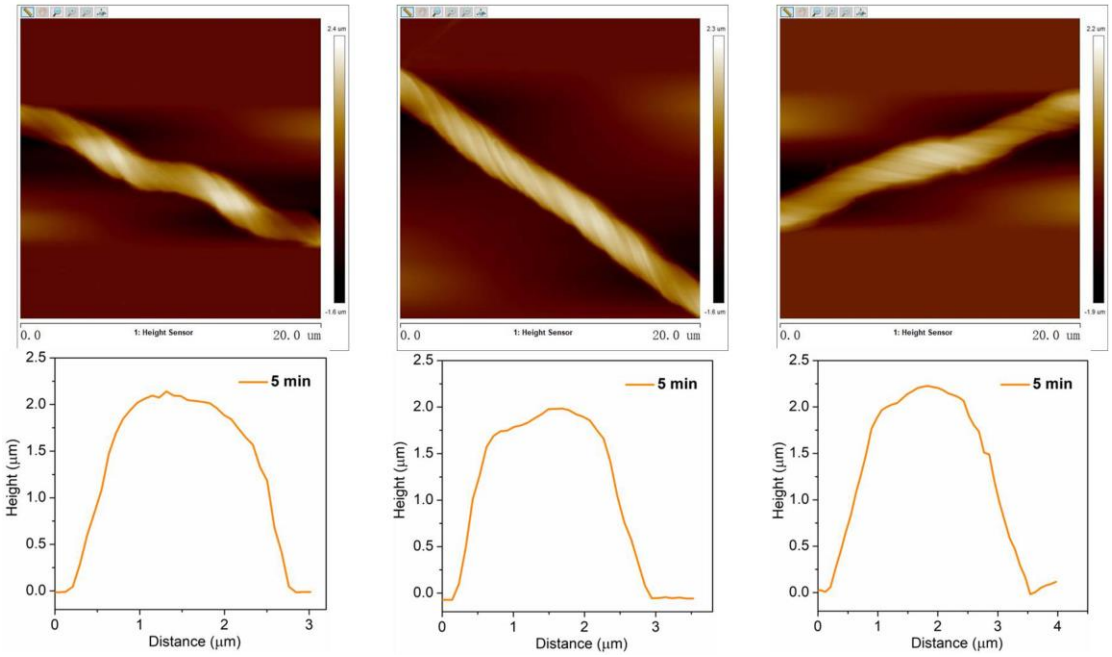

Figure S40. AFM images of ***R*-1h** after immersing in $CHCl_3$ for 5 min (concentration 0.12 mmol/L).

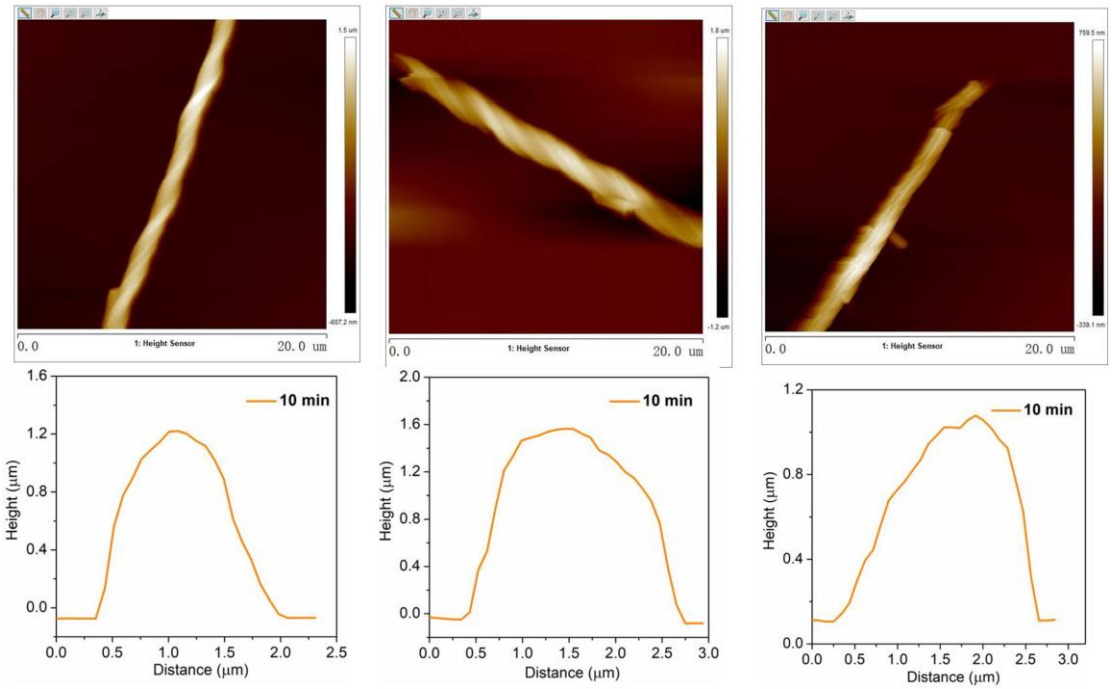

Figure S41. AFM images of ***R*-1h** after immersing in $CHCl_3$ for 10 min (concentration 0.12 mmol/L).

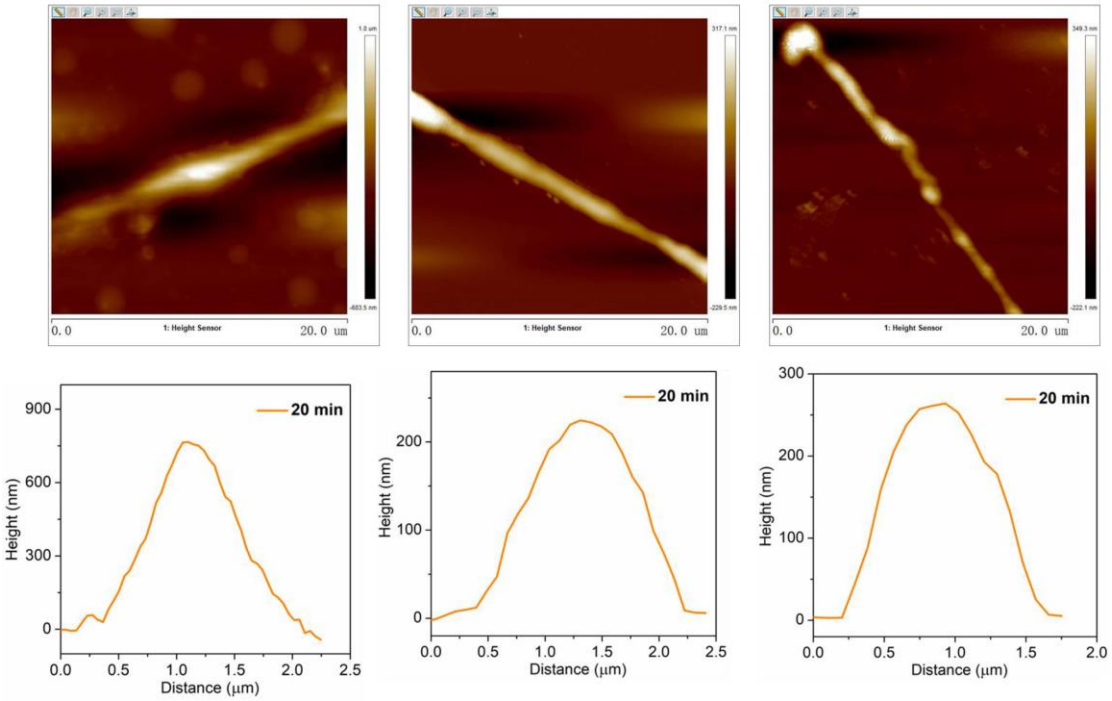

Figure S42. AFM images of ***R*-1h** after immersing in $CHCl_3$ for 20 min (concentration 0.12 mmol/L).

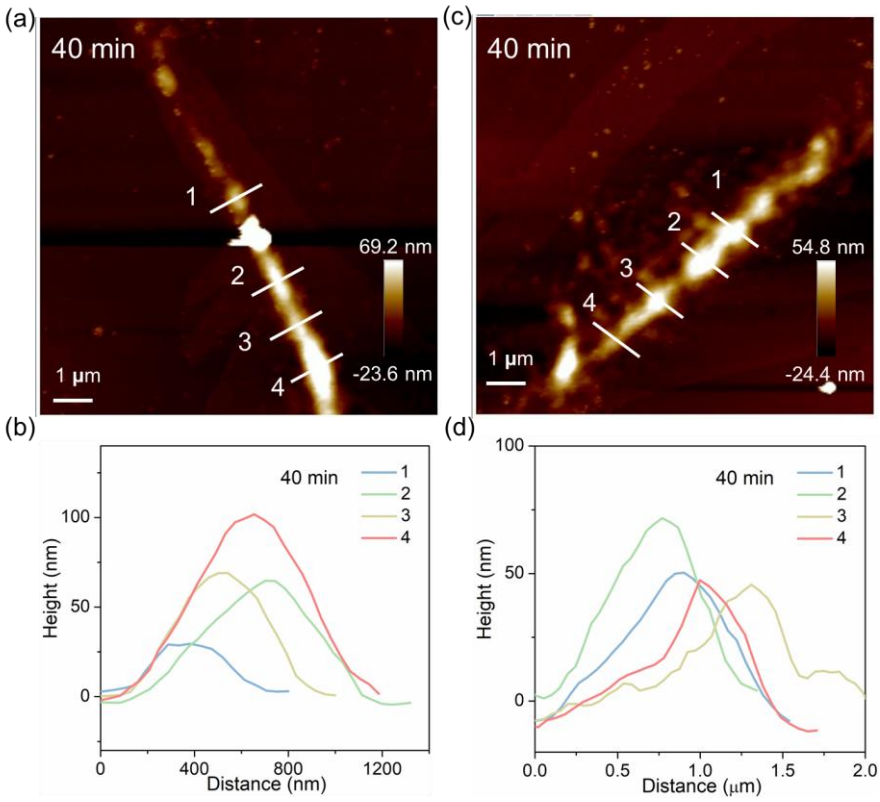

Figure S43. (a, c) AFM images of ***R*-1h** dispersed in $CHCl_3$ (0.12 mmol/L) for 40 min. (b, d) The corresponding height profiles measured along the indicated lines.

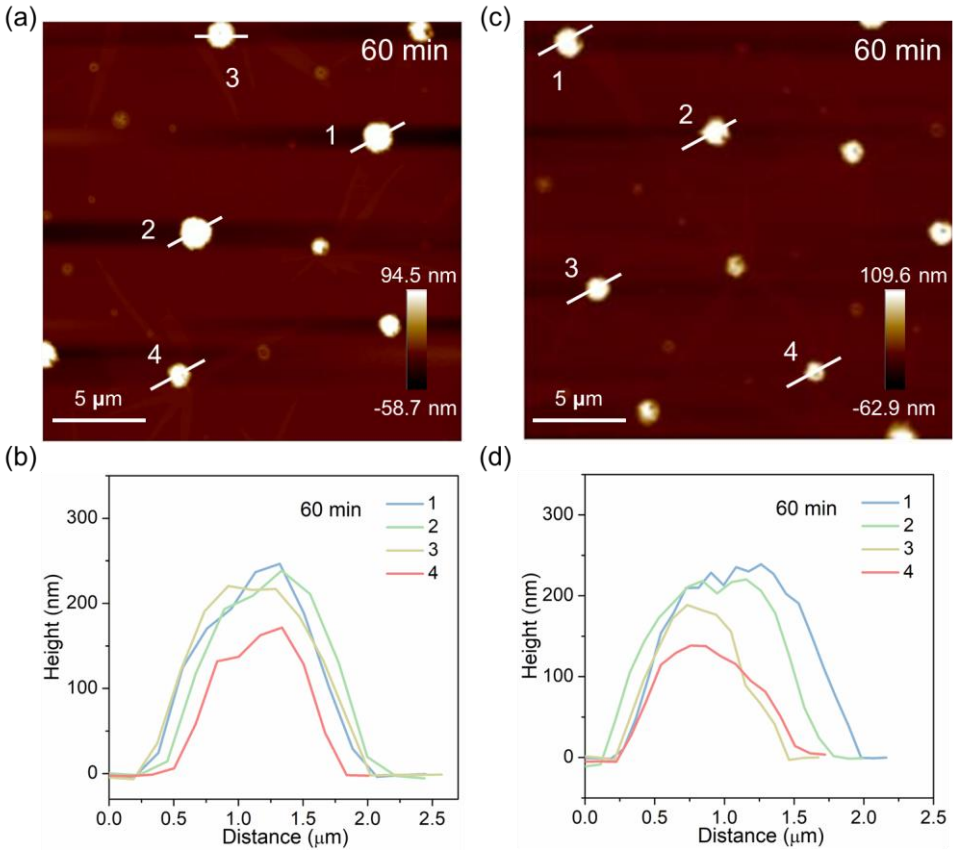

Figure S44. (a, c) AFM images of ***R*-1h** dispersed in $CHCl_3$ (0.12 mmol/L) for 60 min. (b, d) The corresponding height profiles measured along the indicated lines.

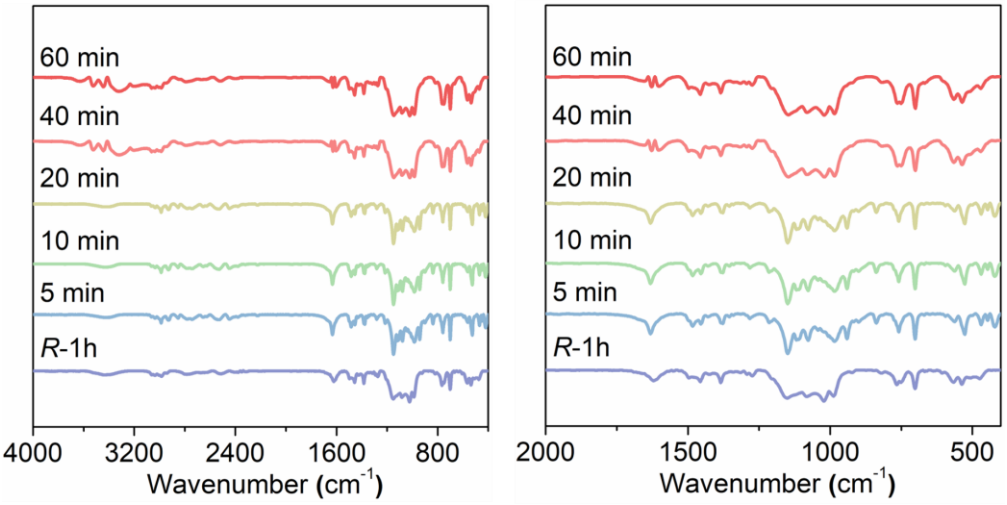

Figure S45. The IR spectra of the solid residue obtained after solvent evaporation of the products formed by immersing ***R*-1h** in $CHCl_3$ for 5, 10, 20, 40 and 60 min (concentration 0.12 mmol/L).

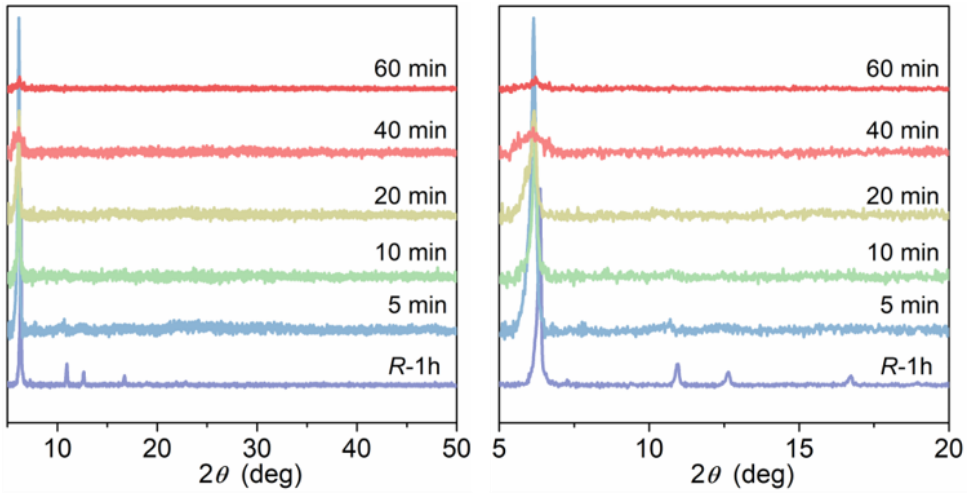

Figure S46. The PXRD patterns of the solid residue obtained after solvent evaporation of the products formed by immersing ***R*-1h** in $CHCl_3$ for 5, 10, 20, 40 and 60 min (concentration 0.12 mmol/L).